HHS Public Access

Author manuscript

J Pharmacol Sci. Author manuscript; available in PMC 2015 August 10.

Published in final edited form as:

J Pharmacol Sci. 2014 ; 125(1): 6–38.

Modern Perspectives on Numerical Modeling of Cardiac Pacemaker Cell

Victor A. Maltsev[1,*], **Yael Yaniv**[1], **Anna V. Maltsev**[2], **Michael D. Stern**[1], and **Edward G. Lakatta**[1]

[1]Laboratory of Cardiovascular Science, Intramural Research Program, National Institute on Aging, NIH, 251 Bayview Blvd, Baltimore, MD 21224-6825, USA

[2]Department of Mathematics, University of Bristol, University Walk, Bristol, BS8 1TW, U.K.

Abstract

Cardiac pacemaking is a complex phenomenon that is still not completely understood. Together with experimental studies, numerical modeling has been traditionally used to acquire mechanistic insights in this research area. This review summarizes the present state of numerical modeling of the cardiac pacemaker, including approaches to resolve present paradoxes and controversies. Specifically we discuss the requirement for realistic modeling to consider symmetrical importance of both intracellular and cell membrane processes (within a recent “coupled-clock” theory). Promising future developments of the complex pacemaker system models include the introduction of local calcium control, mitochondria function, and biochemical regulation of protein phosphorylation and cAMP production. Modern numerical and theoretical methods such as multi-parameter sensitivity analyses within extended populations of models and bifurcation analyses are also important for the definition of the most realistic parameters that describe a robust, yet simultaneously flexible operation of the coupled-clock pacemaker cell system. The systems approach to exploring cardiac pacemaker function will guide development of new therapies, such as biological pacemakers for treating insufficient cardiac pacemaker function that becomes especially prevalent with advancing age.

Keywords

Cardiac pacemaker; sinoatrial node cell; numerical modeling; calcium; ion channels

1. Introduction

Numerical modeling is an indispensable tool of the modern science. Intertwining experimentation and theoretical studies is an important driving force of our exploration of complex biological phenomena. In many cases, numerical modeling is the only feasible way to accurately interpret experimental data describing a complex biological system, whose behavior could be counterintuitive. Furthermore, numerical modeling extends our exploratory horizons beyond experimental data, provides novel mechanistic insights, and

*Corresponding author: Victor A. Maltsev, MaltsevVi@mail.nih.gov.

helps in assessing the actions of drugs (1, 2). Failure of a model to explain novel experimental data requires a shift in the existing paradigm, brought on by creative minds that put forward new theories and new hypotheses to be tested. A pioneer of cardiac cell modeling, Denis Noble noted “We often learn as much from the failures as from the successes of mathematical models.” (3).

Cardiac impulse initiation, the fundamental biological phenomenon indispensable for heart function and life, has been traditionally explored by both numerical modeling and experimental approaches. The present understanding of cardiac pacemaker function has evolved (and continues to evolve) through several paradigm shifts. In 2006 in this journal, we had systematically reviewed (4) the major milestones of the evolution from Galvani and Bernstein, Bozler and Weidman, Noble and DiFrancesco, to our Ca^{2+}-clock hypothesis. The evolution of thought regarding cardiac pacemaker cell function switched back and forth between intracellular origin (e.g. a “metabolic” intracellular clock (5) or sarcoplasmic reticulum (SR)-based Ca^{2+}-clock (4)) and cell membrane origin of heartbeat initiation (membrane clock or M-clock (6)). While the ability of the SR to generate oscillatory Ca^{2+} releases was discovered long time ago ((7), review (8)), the intracellular Ca^{2+} oscillator had been considered mainly as a pathological phenomenon in pacemaker cells; thus an important milestone of 1990s to early 2000s was the recognition of its contribution into NORMAL pacemaker function (9). A more recent paradigm shift was the realization that both intracellular and cell membrane initiation mechanisms are actually tightly dynamically coupled to each other and are indispensable for normal pacemaker function that led to the idea of a “coupled-clock” system (10) (Fig.1A, for more details see review (11)).

This article is the first systematic review dedicated to numerical modeling of pacemaker cell function based on the coupled-clock theory. It summarizes the present state of numerical modeling of the cardiac pacemaker cell as the coupled-clock system. In addition to the two coupled clocks, we also review new emerging numerical modeling approaches which include local Ca^{2+} control, mitochondrial function, biochemical regulation of cAMP production, and protein phosphorylation that drive the pacemaker coupled clock function. We also discuss existing controversies and suggest how these might be resolved in future studies. Because we have broadly and systematically reviewed the evolution of pacemaker mechanisms (4), this critical review discusses only those limited historical aspects that help in resolving existing controversies. Some sections are accompanied by “mini-summaries” that recap major ideas that we believe are important for realistic numerical modeling of cardiac pacemaker cells and may provide a new framework for future work.

2. Basic concepts: Cardiac pacemaker cells and the Diastolic Depolarization (DD)

Pacemaker cells within the heart that have “Clocks” with the briefest rhythmic periods “capture” or trigger other excitable cells. Sinoatrial node cells (SANC) are the dominant cardiac pacemaker cells, because they exhibit shorter periods between spontaneous action potential (APs) than do atrioventricular nodal cells or His-Purkinje cells. Thus, SANC normally initiate the cardiac impulse by generating spontaneous APs that are conducted to the ventricle and entrain the duty cycle of ventricular myocytes.

Different types of heart cells, i.e., pacemaker cells within the sinoatrial node and contractile ventricular myocytes within myocardium, determine the rate and strength, respectively, of the heart beat. During diastole the myocytes maintain their resting potential close to the K^+ equilibrium potential of −90 to −80 mV. In contrast, the heart's pacemaker cells generate spontaneous rhythmic changes of their membrane potential, known as the slow diastolic depolarization (DD) that starts from the maximum diastolic potential (MDP) of about −65 mV. When the membrane potential (V_m) reaches an excitation threshold of about −40 mV, the pacemaker cell spontaneously generates the next AP (blue curve in Fig.1B).

3. A modern view on the cardiac pacemaker mechanism: a coupled clock system

A modern perspective considers SANC, *per se*, as a system, comprised of several levels of complexity and integrated intracellular and cell membrane components (Fig.1A) resulting in coupled electrical and intracellular Ca^{2+} signals (Fig.1B–D) required for normal pacemaker function. Figure 2 shows the dynamic interplay of major ion currents and Ca^{2+} signal dynamics predicted by a contemporary numerical SANC model (discussed below) that embraces many of these interactions.

3.1. Membrane clock

The ensemble of electrogenic molecules within the cell membrane (i.e. ion channels and ion transporters, Fig.1A in blue) imparts the ability of the pacemaker cell to generate DD and rhythmic APs (i.e. automaticity). When activation and inactivation kinetics of the cell membrane ion channels are described by Hodgkin-Huxley (H-H) gating mechanism and assembled together within a context of numerical models in different combinations and contributions, they are able to generate DD and pacemaker potentials observed experimentally. This subsystem of sarcolemmal molecules forming a voltage membrane oscillator was conceptualized as a membrane clock (4) (M-clock, for short). The first M-clock-based pacemaker cell model was developed in 1960 by Denis Noble (6), and it included only two voltage-gated currents (a fast inward Na^+ current and a slow, delayed rectifier K^+ current I_K) and a hypothetical time-independent, leak-like Na^+ background current ($I_{b,Na}$). In this first simple model the DD was generated by the inward-going $I_{b,Na}$, as the conductance of outward-going I_K underwent a time-dependent decay (dubbed the "g_K" mechanism). Inspired by the H-H theory, a multitude of extensive voltage-clamp studies identified and characterized specific sarcolemmal ion currents. Table 1 summarizes the properties of major currents found in SANC. Interested readers are referred to excellent reviews (38, 39) to learn further details of specific properties of each current, including selectivity, conductance, complex gating schemes, and, when known, their molecular basis. Based on the gating schema of the currents, numerous numerical models have been developed and until recently have dominated the cardiac pacemaker field for several decades. For example, the pacemaker M-clock has been the predominant feature in at least 12 SANC numerical models (40). Major M-clock mechanisms include the aforementioned g_K decay mechanism, hyperpolarization-activated funny current (I_f) (41), T-type Ca^{2+} current (I_{CaT}) (14–16), L-type Ca^{2+} current (I_{CaL}) (14), and a sustained inward current (I_{st}) (26). (Please note that I_{st} is different from another current called sustained outward current

I_{sus}, that is 4-amonpyridine-sensitive component of I_{to}). The most recent update on numerical modeling of I_f was published by Verkerk and Wilders (42).

It has been later realized, however, that a direct application of the H-H approach to understanding the cardiac pacemaker function is problematic and insufficient (10, 43, 44). M-clock-based models fail to reproduce many experimental results, especially a substantial AP firing rate reduction or a cessation of automaticity of pacemaker cells produced by specific inhibition of Ca^{2+} cycling (9, 32, 33, 45, 46) or PKA-dependent phosphorylation (47). These experimental results, however, are reproduced by novel numerical modeling (described below), in which M-clock mechanisms do not operate in isolation, but dynamically interact with intracellular signaling, i.e. within the complex integrated system of intracellular and cell membrane proteins, as shown schematically in Figure 1A. We believe that realization and validation of these two-way symbiotic interactions (marked "Yin-Yang" in Fig.2) is the key to resolving many existing controversies within the cardiac pacemaker field (discussed below in Section 5).

Mini-summary

- **a.** The ensemble of ion currents generated by electrogenic proteins of cell surface membrane is defined as the M-clock.
- **b.** While the ion currents are the immediate cause of any membrane potential change, they are dynamically modulated by rhythmic intracellular signaling.
- **c.** Despite the fact that the M-clock generates perfect pacemaker potentials *in silico* and has been considered as the dominant pacemaker mechanism for more than 50 years, numerical models based mainly on M-clock cannot explain recent experimental results and become obsolete.
- **d.** Modern numerical modeling includes emerging powerful intracellular pacemaker mechanisms dynamically coupled to M-clock.

3.2. Calcium-clock

A powerful intracellular pacemaker mechanism is linked to the SR, a major Ca^{2+} store in cardiac cells. It has a molecular Ca^{2+} pump (SERCA) and Ca^{2+} release channels (ryanodine receptors, RyRs) and, when Ca^{2+} is available, is capable of generating almost periodic, rhythmic Ca^{2+} oscillations, independent of cell surface membrane function (7, 48). Thus, the SR has been conceptualized as a Ca^{2+} clock (in grey in Fig.1A) (4). The Ca^{2+} clock is active in the basal state in cardiac pacemaker cells and contributes to their DD via multiple Ca^{2+} dependent processes embodied within the cell surface membrane.

Specifically, Ca^{2+} clock generates localized diastolic Ca^{2+} releases (dubbed Local Ca^{2+} Releases or LCRs, Fig.1B) in pacemaker cells in the absence of Ca^{2+} overload as documented in confocal imaging of Ca^{2+} dynamics in mammalian SANC and atrial subsidiary pacemaker cells combined with non-invasive perforated patch-clamp electrophysiology (35, 49). These LCRs are initiated beneath the cell surface membrane during DD via spontaneous activation of RyR. In confocal line-scan recordings, LCRs appear as 4–10 μm Ca^{2+} wavelets during and following the dissipation of the global systolic

transient effected by the prior AP, and crescendo during the DD, peaking during the late DD, as they merge into the global cytosolic Ca^{2+} transient triggered by the next AP. A high-speed camera detects from 8 to 27 (13 on average) LCRs per cycle during spontaneous AP firing by rabbit SANC, with the LCR size increasing as DD progresses from the MDP to the AP threshold (50). The individual diastolic LCRs form an ensemble Ca^{2+} signal (i.e. integral of all LCRs, Fig.1C,D) reported in single pacemaker cells of numerous species (35, 49, 51–55). Joung et al. (56) coined the term "Late Diastolic Ca^{2+} Elevations" (LDCaE) for this LCR-generated signal when it was found in SA node tissue (56, 57).

LCR occurrence does not require triggering by depolarization of the surface membrane: persistent rhythmic oscillatory membrane currents can be activated by rhythmic LCRs during voltage-clamp (at potentials that prevent cell Ca^{2+} depletion, e.g. −10 mV) (48). Both persistent LCRs and the net membrane current exhibit simultaneous fluctuations of the same frequency (47, 48), and both are abolished by ryanodine (58). Sustained LCR activity is also observed in chemically "skinned" SANC (i.e. having a detergent-permeabilized cell surface membrane) bathed in a physiological $[Ca^{2+}]$ of 100 nM (47, 48). LCRs are generated as rhythmic events at rates of 1 to 5 Hz, i.e. encompassing those of spontaneous AP firing in SANC. In the absence of β-Adrenergic Receptor (β-AR) stimulation (i.e. in the basal state) the Ca^{2+} clock is present and operative in the pacemaker cells, but not in contractile cardiac muscle cells under normal conditions. Rhythmic LCRs occur not because of an elevated intracellular $[Ca^{2+}]$ (minimal diastolic $[Ca^{2+}]$ is low, ~160 nM, in SANC (48)) but because phosphorylation of Ca^{2+} cycling proteins is enhanced in these pacemaker cells (47), whereas phosphorylation state of these proteins in the muscle cells is suppressed (59).

Mini-summary

- **a.** An SR-based "Ca^{2+} clock" is a fundamental property of cardiac cells.
- **b.** During spontaneous AP firing, SR of SANC generates two major Ca^{2+} releases: one is the AP-induced Ca^{2+} transient via classical Ca^{2+}-induced Ca^{2+} release (CICR) mechanism and the other is the LCR mechanism during DD.
- **c.** LCRs are driven by enhanced pumping and release due to an enhanced phosphorylation state of SR Ca^{2+} cycling proteins and free Ca^{2+} available for cycling (i.e. oscillatory substrate).

3.3. The coupled-clock system: its interactions and phosphorylation-driven mechanism

Interaction of the clocks occurs throughout the entire pacemaker cell duty cycle. During DD, the ensemble LCR signal (i.e. LDCaE) activates inward I_{NCX} that accelerates DD and "ignites" the next AP (Fig.2, "AP ignition"). Thus, the timing of this acceleration is crucial for the cycle length and therefore for the beating rate under given conditions. This crucial timing has been characterized in terms of the LCR period, determined as the delay between the AP-triggered global cytosolic Ca^{2+} transient and LCR emergence during DD ("LCR period" in Figs 1B, 2).

The most recent paradigm shift in our understanding of cardiac pacemaker function was the realization that while LCRs are generated by the SR (i.e. by the Ca^{2+} clock), the LCR period

is not an exclusive property of the SR, but it reflects the functional state of the entire system that also includes ion currents of the M-clock. As a matter of fact, the LCR period is regulated not only by the kinetics of SR Ca^{2+} pumping and release, but also by the quantity of intracellular Ca^{2+} made available for pumping into the SR via sarcolemmal Ca^{2+} flux (Fig.2, “refueling”) which is regulated by membrane ion channels and transporters. The contributions of L-type Ca^{2+} channels (LCCh) and NCX to the Ca^{2+} balance and, hence, LCR period are obvious. But K^+ channels, and even funny channels (I_f panel in Fig.2), are also indirectly implicated in the Ca^{2+} balance: K^+ channels repolarize membrane potential to deactivate LCCh and to activate I_{NCX}, and funny channels limit hyperpolarization and, hence, Ca^{2+} efflux via NCX. Thus, the LCR period embraces complex interactions of cell membrane electrogenic molecules and intracellular Ca^{2+} cycling molecules (Fig.1A) and is a “readout” of the restitution kinetics that define the “ticking speed” of the coupled-clock system.

While individual wavelet-like LCRs exhibit a degree of stochasticity in their occurrence, they form LDCaE that appears fairly synchronously and rhythmically, i.e. approximately at the same time during DD, determined (on average) by the functional state of the complex protein phosphorylation regulatory network (Fig.1A) in a given steady-state condition. A major feature of this network is a relatively high level of basal cAMP (47) and PKA-dependent and CaMKII-dependent phosphorylation of proteins in SANC (both in SR and cell membrane) that is achieved due to a high constitutive level of activation of adenylyl cyclases (ACs) that drives spontaneous LCRs.

Although SANC, like ventricular myocytes, express high levels of Ca^{2+}-inhibited AC types 5 and 6 (60), the discoveries of Ca^{2+}-activated AC types, i.e. AC1 and AC8, in rabbit and guinea-pig SANC (61, 62) and localization of the basal Ca^{2+}-activated AC activity within lipid raft microdomains (62) link Ca^{2+} to localized cAMP production (Fig.1A). Ca^{2+} binds to calmodulin to activate AC, leading to a high basal level of cAMP-mediated, PKA-dependent phosphorylation of surface membrane and intracellular proteins involved in cell Ca^{2+} balance and SR Ca^{2+} cycling (47, 62) (Fig.1A).

Steady levels of activation of the effector proteins are ensured, in turn, by mechanisms to damp this complex cAMP-phosphorylation-driven signaling (Fig.1A, red arrows). Basal phosphodiesterase activity is one such restraining mechanism to reduce the high constitutive AC activity in SANC (63). Basal activation of phosphoprotein phosphatases in SANC (64) is another mechanism that limits PKA and CaMKII-dependent phosphorylation. The net result of basal activation of phosphodiesterase and phospho-protein phosphatases is that the basal LCR period and AP cycle length are maintained near the midpoint of their functional ranges. Other restraining mechanisms of the system limit Ca^{2+} influx and hence cell Ca^{2+} load, for example, calmodulin-mediated LCCh inactivation, which limits Ca^{2+} influx via LCCh during each AP. Thus, the robustness of the coupled-clock system is imparted by its numerous functional redundancies and dual regulation of SR Ca^{2+} cycling and membrane ion current generators by a common set of factors (coupling factors or nodes, Fig.1A, purple labels). The system activity is kept in check by “brakes” (Fig.1A, red arrows) represented by phosphodiesterase and phosphatase activities, voltage-dependent negative feedback on ion fluxes and calmodulin-dependent modulation of LCCh.

Mini-summary

a. LCR ensemble signal (LDCaE) during DD activates I_{NCX} that accelerates DD and therefore the LCR timing regulates DD and thus the AP firing rate.

b. Ca^{2+} fluxes via surface membrane proteins regulate intracellular Ca^{2+}, and therefore the LCR period is a property of the entire coupled-clock system, not just a sole function of SR cycling proteins.

c. cAMP, Ca^{2+}, and PKA- and CaMKII- dependent protein phosphorylation, are major regulatory nodes of the coupled system (Fig.1A).

d. The system is restrained from "explosion" by molecular "brakes" (Fig.1A, red arrows) that keep the system regulation under basal condition close to its mid-range.

e. The complex interactions depicted in Figure 1A are the essence of the system's ability to function as a clock, i.e. despite substantial transient cell Ca^{2+} changes during each AP cycle, the steady-state average cell Ca^{2+} balance and levels of phosphorylation of M and Ca^{2+}-clock proteins remain stable, so that all events recur each cycle in same sequence, timing, and magnitude, thus ensuring a stable AP CL.

4. Novel numerical models based on the coupled-clock mechanism

4.1. New insights derived from first coupled-clock model of 2009

First attempts (54, 65) to numerically model LCRs and their ensemble signal (LDCaE in current terminology) used a smooth function, such as a sine function, with a given phase and amplitude, directly mimicking their experimentally measured values. These phenomenological Ca^{2+} release formulations were integrated into a SANC model (such as 2002 Kurata model (66)) that mimicked experimentally observed Ca^{2+} signals in SANC. While this kind of relatively simple modeling demonstrated a capability of Ca^{2+} releases to generate powerful NCX currents contributing to the DD, it remained essentially naive and did not embrace a numerical mechanism of Ca^{2+} "clocking". Next theoretical model of cardiac pacemaker function known as Maltsev-Lakatta model (or ML model) predicted oscillatory LCR signals driven by SR Ca^{2+} pumping and release kinetics. Key predictions of the ML model are shown in Figure 2.

While the ML model originated prior 2002 Kurata et al. model (66), it has many features that have provided (and continue to provide) new insights into cardiac pacemaker cell function. The SR Ca^{2+} release approximation was adopted from formulations suggested earlier by Shannon et al. (67). This model was constructed and optimized based on the results of a wide-scale parametric sensitivity analysis of classic formulations of membrane clock and Ca^{2+} cycling (within 100s of thousands of specific models, see Section 6.1 for details). This approach allowed to find realistic numerical solutions that reproduced the new experimental results.

Specifically the ML model reproduces effects of basal phosphorylation of phospholamban and RyR (47) by enabling higher rates of SR Ca^{2+} pumping and release vs. prior SANC

models and models of cardiac muscle cells. With these fundamental changes, SR indeed becomes a numerical Ca^{2+} oscillator based on a simple *Release-Pumping-Delay* mechanism. The oscillator operates within a broad range of parameters and generates Ca^{2+} releases over a wide range of frequencies (1.3 to 6.1 Hz) that encompass physiological heart rates of many mammalian species.

The integrated Ca^{2+} clock and M-clock within the ML model generates substantial diastolic Ca^{2+} release and I_{NCX}, found previously experimentally (35), but absent in prior models (Fig.3A). Figure 3B shows that diastolic I_{NCX} substantially increases before I_{CaL} activation in the model, but not in Kurata et al. model (66). The ML model faithfully reproduces new experimental results with perturbation of Ca^{2+} cycling (e.g. ryanodine effect) and phosphorylation (e.g. PKA inhibition). Importantly, SR Ca^{2+} clock not only modulates the M-clock, but that the M-clock, in turn, also affects Ca^{2+} clock (Fig.2). Functions of both clocks are simultaneously and dynamically coupled in the model via multiple *coupling factors*, such as Ca^{2+} cAMP, PKA, and CaMKII. Thus, the complex model behavior and regulation are characterized in new terms "*coupling factors*" and "*the coupled clock system*": "*the coupled clock system* is very robust and, importantly and advantageously, also very flexible" (10). Indeed, surprisingly the coupled system exhibited a greater robustness and flexibility than M-clock operating alone (see section 6.1 for details).

Additional numerical model simulations provide further mechanistic insights into the complex SR restitution process and its control of the AP cycle length (Fig.4). The simulations predict the wide range of pacemaker rate regulation via variations in the maximum SR Ca^{2+} pumping rate (P_{up}, reflecting the number of functional SERCA molecules and phospholamban phosphorylation by PKA, 1 to 30 mM/s). In particular, the more rapid the SR Ca^{2+} pumping kinetics, the sooner the SR gets refilled with Ca^{2+} to achieve the threshold required for spontaneous diastolic release (reflected in the ensemble LCR signal, i.e. LDCaE). The earlier Ca^{2+} release at higher P_{up} generates an earlier I_{NCX} which accelerates DD rate at an earlier time, leading to an increase of the AP firing rate. The ML model prediction of the crucial importance of SR Ca^{2+} refilling kinetics for SANC AP firing rate has been confirmed in other numerical modeling studies (43, 68) and also experimentally, specifically by measuring SR Ca^{2+} signals (via a Fluo-5N indicator) (69).

Another interesting prediction of the ML model is that at higher pumping rates the diastolic release occurs not only earlier, but also stronger. This highly synchronized release generates a stronger I_{NCX} that allows to reach the AP threshold in a shorter time (i.e. ensures robust AP ignition).

Mini-summary

a. Classical theoretical models portray SANC pacemaker mechanisms mainly as an M-clock (40). The coupled-clock ML model differs fundamentally from the mainly-M-clock-based models, and uniquely reproduces many experimentally documented features of pacemaker cells.

b. The ML model and its numerous specific “parametric-space” derivatives provide a new framework for further numerical investigation of the coupled-clock pacemaker system to discover the best match for existing and future experimental results.

4.2. Novel interpretation of ivabradine-induced bradycardia

Ivabradine at low concentrations (below 3 μM) specifically inhibits I_f, i.e. it does not directly suppress L-type current (70), SR Ca^{2+} cycling (71) and other surface membrane ion channels (72). A beneficial effect of ivabradine for heart rate reduction has been confirmed in clinical trials (review (73)) and interpreted solely on the basis of I_f inhibition. Within the coupled-clock theory discussed above, however, SANC normal automaticity is regulated by a crosstalk between M-clock and Ca^{2+} clock and, indirect suppression of the Ca^{2+} clock is therefore expected to further contribute to the steady-state ivabradine-induced bradycardia. This interesting hypothesis has been recently tested by Yaniv et al. (71) in rabbit SANC. Indeed, ivabradine-induced slowing of the AP firing rate is accompanied by indirect reduction of SR Ca^{2+} load, slower intracellular Ca^{2+} cycling kinetics, and prolongation of the LCR period.

Numerical model simulations, also performed by Yaniv et al. (71) using the modified coupled-clock ML model (74), provided further insights into the complex ivabradine effects (Fig.5). We predicted that a reduction in I_f indirectly inhibits Ca^{2+} clock: it initiates a reduction in number of APs per unit time that reduces the Ca^{2+} influx per unit time. This reduction in net Ca^{2+} influx results in a reduction in Ca^{2+} available for pumping (because of a reduction in cytosolic Ca^{2+}), reducing the SR Ca^{2+} load and prolonging the period of local Ca^{2+} release. Prolongation of LCR period shifts the Ca^{2+} activation of I_{NCX} to a later time during DD, which further reduces the AP firing rate, leading to further reduction in Ca^{2+} influx per unit time. In other words, inhibition of the Ca^{2+} clock induces further indirect suppression of the M-clock, and so on, until the system reaches a new steady-state bradycardia. Importantly, this entrainment between the two clocks (documented within the context of a coupled-clock numerical model) is required to explain the experimentally verified AP firing rate reduction by ivabradine.

The numerical model predicts that the complex effects of ivabradine do not end with this kind of “biophysical” entrainment, but also include a “biochemical” component. The initial decrease in Ca^{2+} influx decreases Ca^{2+}-activated CaMKII and adenylyl cyclases-cAMP/PKA signaling. The resultant reductions in phosphorylation of Ca^{2+} cycling proteins and membrane proteins further reduce the net Ca^{2+} influx and the SR Ca^{2+} loading and both further reduce AP rate; and, in parallel, the resultant reduction in cAMP further shifts the I_f activation curve. Further numerical model simulations (71) in the absence of this additional “biochemical” crosstalk can account for only about 50% of the experimentally measured reduction in steady-state AP firing rate that occurs in response to ivabradine. The full ivabradine effect can be explained only on the basis of almost equal contributions by the “biophysical” and “biochemical” components.

The bradycardiac effect actually is fully symmetric with respect to the two coupling clocks, i.e. it does not matter of which clock was directly or indirectly perturbed first (71). The LCR period and AP cycle length shift toward longer times almost equally by either direct

perturbations of the M-clock (by ivabradine) or of the Ca^{2+} clock (by cyclopiazonic acid, a specific inhibitor of the SR Ca^{2+} pump). During both perturbations the LCR period reports the crosstalk between the clocks. Based on this finding, the steady-state bradycardia associated with different HCN4 mutations is likely mediated, only in part by I_f inhibition, and in part, by change in Ca^{2+} clock due to the clocks' cross-talk (75). The same is true for mutations of Ca^{2+} regulatory protein (71, 75): only part of the bradycardia effect is explained by a direct change of the Ca^{2+} clock, but the full effect is explained by the coupling of Ca^{2+} clock and M-clock (including e.g. aforementioned cAMP-dependent effect on I_f).

A recently updated ML model by Severi et al. (76), in which I_f amplitude was set substantially larger than in the ML model, can, even with limited crosstalk between the membrane and Ca^{2+} clocks, reproduce the steady-state changes in spontaneous AP firing rate in response to ivabradine (75). However, this model predicts only a modest decrease in SR Ca^{2+} load, which is not in accord with experimental results. Therefore, computational models that predict changes in steady-state spontaneous AP firing rate by ivabradine mainly via changes only in membrane clock (I_f), and not via crosstalk between the clocks are likely not realistic.

Mini-summary—Selective inhibition of either Ca^{2+} clock or M-clock produces …

a. the same effect, i.e. increase in both LCR period and AP firing cl.

b. a suppression of both clocks within this system.

c. a reduction in cAMP/PKA and CaMKII signaling.

4.3. A novel quantitative explanation of autonomic modulation by the coupled-clock theory

Classical numerical models attribute regulation of normal cardiac automaticity in SANC largely to G protein-coupled receptor (GPCR) modulation of sarcolemmal ion currents, specifically I_f, I_{CaL}, I_{Kr}, and I_{Ks} (77). More recent experimental evidence (summarized in (11)), however, indicates that GPCR modulates SANC automaticity over a wide physiologic range, e.g. from 60 to 240 bpm in humans, via variation in GPCR signaling (Fig.1A, green and red shapes) that links both β-AR and ChR to the very same nodes (or coupling factors) of the coupled-clock system (Fig.1A, purple labels, i.e. PKA, CaMKII, cAMP and Ca^{2+}) that regulate basal state LCR period: Stimulation of sympathetic β-Adrenergic Receptor (β-AR) in SANC, via G_s activation, increases the spontaneous AP firing rate via effect on proteins of both clocks. As a result, the enhanced and coupled function of the clocks not only modulates ion channel function (as in classical mechanism), but also modulates diastolic LCRs occurrence (i.e. in earlier and more synchronized and abundant LCR occurrence in rabbit SANC (47)). In contrast, Cholinergic Receptor (ChR) stimulation results in later, rare and less synchronized LCR occurrence (78).

This new experimentally discovered LCR-dependent mechanism of autonomic modulation has been recently explored by using the ML model featuring coupled-clock pacemaker mechanism (43). Ca^{2+} release characteristics in the model were graded by variations in the SR Ca^{2+} pumping capability (P_{up}) by SERCA, but ion channels were simultaneously

modulated as previously reported in voltage-clamp studies. SERCA activity is partially inhibited by phospholamban (Fig.1A). This inhibition wanes and SERCA activity increases when phospholamban becomes phosphorylated via cAMP-dependent PKA signaling. Thus, P_{up} variations in the model mimic, in part, various degrees of phosphorylation of phospholamban by PKA due to autonomic modulation via GPCR and GPCR-activated AC (Fig.1A).

The novel numerical model (43) of pacemaker rate modulation via GPCR is based on numerous complex synergistic interactions between sarcolemmal and intracellular processes via membrane voltage and Ca^{2+}. Major interactions include changes of I_{NCX} that couple the respective changes in phase and amplitude of diastolic Ca^{2+} releases to the DD rate and ultimately to the AP potential firing rate (Fig.6A). Concomitantly, changes in amplitude and frequency of I_{CaL} activation shift cell Ca^{2+} balance to support the respective Ca^{2+} cycling changes.

The model faithfully predicted the entire range of physiological chronotropic modulation of SANC by activation of β-AR or ChR only when experimentally documented changes of sarcolemmal ion channels are combined with a simultaneous increase/decrease in SR Ca^{2+} pumping capability. In contrast, prior models developed by Dokos et al. (79), Zhang et al. (80) and Kurata et al. (66) mainly based on M-clock function do not predict β-AR stimulation effect with experimentally documented changes in I_{CaL}, I_{Kr}, and I_f and doubled SR Ca^{2+} pumping capability (Fig.6B).

Mini-summary

- **a.** Autonomic modulation of AP firing rate by SANC involves changes not only in ion channels but also in Ca^{2+} cycling proteins and both effects are predicted by the coupled-clock numerical model simulations.
- **b.** Ca^{2+} clock is regulated by ion channels via their contribution to cell Ca^{2+} balance.
- **c.** Varying degree of phosphorylation of proteins comprising the coupled-clock system is a key factor in the new mechanism of autonomic modulation of AP firing rate.
- **d.** GPCR signaling translates autonomic modulation to effector proteins of both clocks via the same coupling factors (Ca^{2+} and PKA-dependent phosphorylation) that ensure robust pacemaker cell function in the basal state.
- **e.** This universal (coupled-clock) mechanism confers robustness and simultaneously flexibility to cardiac pacemaker cell system that cannot be achieved by the M-clock alone.

4.4. Kinetics and magnitude of AC-cAMP/PKA signaling

It has been shown that basal, steady-state levels of cAMP and the phospholamban phosphorylation are relatively high vs. ventricular myocytes, and they increase further in response to β-AR stimulation (47) or decrease in response to ChR stimulation (78). However, a realistic numerical modeling of the complex networks of enzymatic cascades

that regulate cardiac pacemaker function (Fig.1A) ought to include kinetic properties of the system components. These, however, remain mainly unknown and require dedicated studies. Specifically, it is important to quantify experimentally and numerically the kinetics of cAMP formation, PKA activation and protein phosphorylation, and their relationships to changes in spontaneous AP firing rate. The cAMP formation rate has been reported by measuring AC activity in suspension of lysates of pacemaker cells (62). The cAMP formation rate turned out to be Ca^{2+} dependent. A recent pilot study by Yaniv et al. (81) has made the first attempt to measure the live kinetics and magnitude of PKA activity in single pacemaker cells. Cultured rabbit SANC were infected with an adenovirous expressing the PKA activity FRET sensor, AKAR and changes in kinetics and magnitude of PKA activity were measured in response to graded β-AR stimulation (using isoproterenol). In parallel, the AP firing rate kinetics were measured in another subset of cells. PKA and AP firing rate kinetics change in parallel in response to different isoproterenol concentrations (Yaniv et al. unpublished observations).

A novel integrative numerical model has been developed based on the ML model to simulate the expected rate of cAMP production and the kinetics and magnitude of protein phosphorylation (81). The model includes previously measured steady-state AC-activity, cAMP and phospholamban phosphorylation levels in response to perturbation that influence cAMP/PKA signaling and the changes in the kinetics and magnitude of PKA activation. In response to maximal β-AR stimulation the model simulations predict that the rate of cAMP generation was slower than that of the experimentally measured PKA activation.

Mini-summary

- **a.** Despite their crucial functional importance (discovered experimentally), the complex networks of enzymatic cascades in pacemaker cells remain basically unexplored numerically.
- **b.** The first coupled-clock numerical model based on recent measurements of PKA kinetics via a FRET sensor, demonstrates that the signaling cascade "Ca^{2+}→CaM→CaM-activated-AC→cAMP→PKA→ phosphorylation" (Fig.1A) regulates the spontaneous AP firing rate of SANC across its entire physiological range.
- **c.** Further progress in numerical studies requires obtaining additional data on kinetics and magnitude of activity of the cAMP/PKA and CaMKII signaling in response to different perturbations.
- **d.** Because both cAMP and phosphorylation signaling are highly compartmentalized, an important aspect of future realistic modeling is regulation of **local** interactions within the enzymatic pathways.

4.5. SANC energetics

Recent studies characterized major mechanisms that control ATP supply and demand in SANC (74, 82, 83). The mitochondrial density and respiration rate (which, in a physiologically coupled mitochondrial system, reflects the rate of mitochondrial ATP production) in SANC are similar to that in electrically stimulated ventricular myocytes at 3

Hz (82). However “the energy budget” is managed differently in the two cell types: the myofilament force production is the major ATP consumer in ventricular myocytes, while in SANC synthesis of cAMP and cell ionic homeostasis (especially Ca^{2+} cycling maintenance) are the major ATP consumers. Moreover, the control mechanisms that match ATP supply to demand in SANC are different from those in ventricular myocytes. In ventricular myocytes cytosolic Ca^{2+} enters mitochondria through the mitochondrial uniporter (84) and is extruded by the mitochondrial NCX (85). Changes in mitochondrial Ca^{2+} in these cells alter the activity of several mitochondrial enzymes that take part in ATP production (see review (86)). In contrast to ventricular myocytes, in which Ca^{2+} and ADP/Pi directly signal to the mitochondria to regulate basal state ATP supply (for review cf (87)), in SANC a reduction of Ca^{2+} influx into the mitochondria does not significantly alter the ATP level in the basal state. Instead, Ca^{2+}-calmodulin activation of cAMP/PKA and CaMKII signaling in SANC has a major role to link basal ATP utilization and mitochondrial ATP production: a gradual reduction in cAMP/PKA (82) and/or CaMKII (74) signaling is accompanied by gradual reduction in ATP and a reduction in AP firing rate. At high ATP demand, however, both Ca^{2+} directly and indirectly, via calmodulin activation of cAMP/PKA and CaMKII signaling, control ATP supply to demand matching (83).

Mini-summary

- **a.** Future modeling approach should include ATP production mechanisms and the limit of available ATP at low demand.
- **b.** The Ca^{2+}-activated-cAMP/PKA signaling cascade that drives spontaneous AP firing of SANC is a unique core feed-forward system, that not only drives the basal ATP consumption but also regulates the ATP production. Therefore, numerical models of cAMP/PKA signaling should also include this signaling to mitochondrial ATP production.
- **c.** A decease in spontaneous AP firing rate is associated with decrease in the ATP level.
- **d.** Although only a prototype model exists to correctly describe the ATP energetics balance in SANC (88), future models that attempt to describe the effect of reduction in cAMP/PKA and CaMKII signaling on spontaneous AP firing rate should take into account that ATP may not be available to ATP-dependent mechanisms (e.g., Na^+/K^+ATPase, SERCA pump) and that part of the reduction in spontaneous AP firing rate is due to lack of available ATP.

4.6 Mitochondria in SANC dynamically buffer cytosolic Ca^{2+}

Similar to ventricular myocytes, mitochondrial Ca^{2+} flux in SANC plays a fundamental role in buffering cytosolic Ca^{2+} and modulates SR Ca^{2+} load under normal conditions (74). And therefore it must indirectly affect SR Ca^{2+} release (Fig.7). Recent experimental studies have shown that, indeed, an increase in mitochondrial Ca^{2+} by inhibition of mitochondrial NCX also decreases the SR Ca^{2+} load and as expected on the basis of coupled-clock theory, reduces the ensemble LCR Ca^{2+} signal (74). In contrast, a reduction in mitochondrial Ca^{2+} by inhibition of the mitochondrial uniporter increases the SR Ca^{2+} load and increases

ensemble LCR Ca^{2+} signal. Therefore, changes in Ca^{2+} cycling into and out of mitochondria in SANC modulate basal coupled-clock system automaticity.

To quantitatively simulate SR and mitochondrial dynamics, surface membrane currents and AP firing rate when mitochondrial Ca^{2+} is perturbed, the SANC coupled-clock numerical model (10) was extended to include mitochondrial Ca^{2+} fluxes (74). Simulations of the extended coupled-clock numerical model predicted both systolic and diastolic levels of mitochondrial [Ca^{2+}], whereas experimental data do not permit quantification of these levels, rather only an average level of mitochondrial [Ca^{2+}] can be measured (using Mn^{2+} quench technique (74)). Moreover, the model simulations predict that the major M-clock component that induces change in spontaneous AP firing rate when mitochondrial Ca^{2+} is perturbed is the sarcolemmal NCX, due to changes in its current kinetics altered indirectly by changes in LCR characteristics.

Mini-summary

- **a.** Changes in Ca^{2+} cycling into and out of mitochondria in SANC modulate basal coupled-clock system automaticity via an impact on cell Ca^{2+}, SR Ca^{2+} loading and on the SR Ca^{2+} release characteristics.
- **b.** This mitochondrial Ca^{2+}-SR Ca^{2+} crosstalk is important for SANC pacemaker function. A prototype numerical model has recently been devised (74).

5. Controversies, unsolved problems and their possible solutions

5.1. Asymmetric interactions of M-clock and Ca^{2+} cycling in earlier models

Historically, the first Noble model of 1960–1962 (6, 89) and MNT models (90) had fixed ion concentrations, and could not describe Ca^{2+} dynamics. In the early 1980s this problem was approached by including formulations for ion concentrations in their pacemaker models (Noble 1984 (91)). This move followed basically an approach undertaken earlier by Beeler and Reuter in 1977 (92) to introduce [Ca^{2+}] into AP model of a ventricular myocyte. While the upgraded Purkinje cell model [DiFrancesco-Noble model of 1985 (93)] and its SANC modification [Noble-Noble model of 1984 (91)] included Ca^{2+} dynamics, precise studies on Ca^{2+} dynamics in pacemaker cells have not been performed until very recently, so that the model formulations were chosen mainly to simply reproduce AP-induced Ca^{2+} transient, similar to ventricular myocytes. Specifically, describing their model, DiFrancesco and Noble wrote “There are too many arbitrary factors and, in any case, the major issue of whether Ca^{2+} release is Ca^{2+}-induced or voltage-induced (or, perhaps, both) is still controversial. Our purpose here is therefore largely limited to reproducing the known [Ca]i transient time course… Even a primitive model, here, is much better than no model at all. “

In their recent article “Competing oscillators in cardiac pacemaking: historical background” (94), Noble et al., while accepting the idea that mutual entrainment of the intracellular Ca^{2+} oscillator and surface membrane oscillator (Ca^{2+} clock and M-clock in our terminology) controls normal automaticity of the heart’s pacemaker cells, attempted to make the case that these oscillators are asymmetric. Specifically, the authors claim that the surface membrane voltage oscillator operates independently of the intracellular SR Ca^{2+} oscillator. Further they

contended that the membrane oscillator can maintain its normal function in the absence of the intracellular Ca^{2+} oscillator. In our opinion, in silico simulations of sinoatrial node cell function in the context of older numerical models, like the 1984 model, that lead to the idea of asymmetry within the coupled membrane-Ca^{2+} oscillator system (with membrane oscillator dominance) are not realistic because a plethora of robust experimental data assembled by numerous investigators demonstrates that the membrane oscillator in pacemaker cells cannot function normally without the intracellular Ca^{2+} oscillator. When intracellular Ca^{2+} cycling is disrupted, the generation of spontaneous AP firing becomes substantially slow, dysrhythmic, or ceases altogether (see review (11)). In contrast, in silico, in the original 1984 model (publically available at CellML.com) complete inhibition of SR Ca^{2+} release (i_rel=0) has little effect on AP firing rate or rhythm (the in silico rate actually slightly increases, rather than decreases). A major reason that the membrane oscillators in such models continue to fire APs in the absence of intracellular Ca^{2+} cycling may be because these are artificially wired to beat spontaneously, by incorporation of parameters that guarantee sustained spontaneous activity into the model's formulation. (Of note, a large collection of these parameters had been available to modelers from numerous experimental voltage clamp data obtained prior to the realization of the importance of intracellular Ca^{2+} cycling). Thus, these older pacemaker models have a built-in asymmetry by their design and thus cannot prove an asymmetry of the real pacemaker cells.

The reason for failure of the 1984 model and others like it to reproduce the robust experimental data regarding the crucial role of intracellular Ca^{2+} cycling in pacemaker cell function becomes apparent when one takes into account that these experimental data robustly demonstrate that SR Ca^{2+} release occurs at two specific times within each SANC AP cycle (see mini-summary for section 3.2 item b) 1) spontaneously, during DD, i.e. before AP upstroke; and 2) in response to the AP-induced activation of L-type channels that trigger SR Ca^{2+} release. The 1984 model portrays **only** the latter Ca^{2+} release, i.e. that in response to the AP, and thus lacks a formulation for Ca^{2+} release or its attendant activation of NCX current during DD. In essence, the 1984 model represents a classical model of excitation-induced Ca^{2+} release as it happens in ventricular muscle cells, and thus does not capture the essence of the hypothesis, based upon the experimental data, of coupled-clock pacemaker system (11).

Nonetheless, in their review (94) Noble et al. insist that NCX current in the 1984 model simulations is indeed activated during DD prior to activation of voltage-gated L-type Ca^{2+} current. A careful examination of their Figure 2 in that paper, however, reveals that, in contrast to the experimental result at −44 mV (left top panel) of Brown et al.(95), the model-simulated NCX current (right bottom panel) appears only at a much higher voltage (about −30 to −28 mV, dashed lines), i.e. during the AP upstroke, following the completion of the spontaneous DD (left bottom panel). Furthermore, application of the original 1984 model (publically available at CellML.com) for the simulations of experimental data at −44 mV (left top panel) fails to reproduce a notable NCX current peak (not shown). This is not surprising because in the original report of their data (95) Brown et al. explicitly state that "The results and computer reconstructions convince us that the i_{si} current is composed of two components: the slower of these, i_{NaCa}, may be inward (sodium) current associated with

electrogenic sodium-calcium exchange. This is **preceded and apparently triggered by** a gated component, $i_{Ca,f}$ (*L-type Ca^{2+} current in current terminology*) which has much faster kinetics". In other words, the role for intracellular Ca^{2+} release as portrayed in asymmetric numerical models which dominated the pacemaker field in 1984, was that Ca^{2+} current triggers Ca^{2+} release (CICR), as it normally does in cardiac ventricular muscle.

As we discussed above, in contrast to the asymmetric nature of the pacemaker's coupled oscillators based upon 1984 model simulations detailed by Noble et al. (94), recent numerical modeling (10) of experimental data points to the idea that the cardiac pacemaker cell is, in fact, a system of symmetrically entrained, inter-dependent oscillators. In other words, during spontaneous AP firing, on a cycle-to-cycle basis, the Ca^{2+} oscillator entrains the membrane oscillator by generating spontaneous rhythmic NCX current, prompting the generation of the next AP; but in doing so, loses Ca^{2+} (its "fuel") via Ca^{2+} efflux by NCX. The resultant AP generated by the membrane oscillator, however, injects sufficient Ca^{2+} into the cell during each cycle to replace lost Ca^{2+} and maintains steady-state SR Ca^{2+} load and Ca^{2+} oscillator function. During voltage clamp near the maximum diastolic potential regularly occurring APs do not occur and the cell and SR lose Ca^{2+} via NCX. In this case, the SR becomes relatively Ca^{2+} depleted (48). Spontaneous Ca^{2+} oscillations become damped and die out, because the entrained Ca^{2+} oscillator, like an engine of a car, stops running when its fuel runs out. In order to examine the true oscillatory properties of the intracellular Ca^{2+} oscillator in the absence of APs, the Ca^{2+} available for SR to pump must be maintained, e.g. by voltage clamping near reversal potential of NCX (to minimize Ca^{2+} loss) or by surface membrane permeabilization, which permits clamping $[Ca^{2+}]$ at a given level (11). Data gleaned from such experiments in which Ca^{2+} is maintained constant clearly demonstrate that SR generates sustained, rhythmic local Ca^{2+} releases (10, 11).

Mini-summary

- **a.** The asymmetry of the Ca^{2+} and voltage oscillators in the older models was built-in by the modelers due to large freedom in choosing model parameters in the absence of relevant experimental data at the time.
- **b.** While older pacemaker cell models, like Noble 1984 model (91), include formulations for Ca^{2+} cycling and reproduce AP-induced Ca^{2+} transient, they fail to reproduce pacemaker-cell-unique diastolic Ca^{2+} release and its associated diastolic I_{NCX} that **precede** I_{CaL} activation and AP upstroke (Fig.3).
- **c.** Recent models based on the coupled-clock mechanism and new data obtained by modern experimental and numerical techniques suggest that Ca^{2+} clock and M-clock are equally, i.e. symmetrically, important for normal cardiac pacemaker cell function due to their dynamic (beat-to-beat) interactions (see below).

5.2. The problem of "Ca^{2+} overload" traditionally associated with pathological conditions

The issue of Ca^{2+} overload in cardiac cells has been previously extensively discussed in our 2006 review in this journal (4). However, the Ca^{2+} overload still remains an issue in the literature as far as the coupled-clock pacemaker concept is concerned. Noble et al. (94), point out that a crucial feature of the coupled-clock M-L model (10), i.e. NCX activation by

spontaneous diastolic Ca^{2+} release prior to the next AP upstroke, shows “similarities to delayed afterdepolarization” (or DAD). Yes, indeed. Originally, DADs had been interpreted as a pathological or abnormal phenomenon because these were provoked by poisoning Na/K pump of Purkinje fibers that resulted in marked Ca^{2+} overload. However, in SANC the occurrence of LCRs that contribute to DD during each diastole are physiologic (not associated with Ca^{2+} overload). As discussed above, the minimal diastolic Ca^{2+} levels in pacemaker cells are low, ~ 160 nM (48), i.e. similar to the diastolic Ca^{2+} levels in ventricular myocytes under normal conditions. The spontaneous LCRs are driven instead by a high basal state of phosphorylation of Ca^{2+} cycling and cell membrane proteins, rather than Ca^{2+} overload. These fundamental features of cardiac pacemaker cells are absent in older numerical models, like the 1984 model, and have been modeled only more recently (10, 43).

Mini-summary

- **a.** Partially synchronized, spontaneous Ca^{2+} releases, which are abnormal for cardiac muscle cells, are required for normal function of cardiac pacemaker cells.
- **b.** The spontaneous LCRs occur in pacemaker cells due to enhanced phosphorylation mechanism in the absence of Ca^{2+} overload.

5.3. Controversy regarding effects of cytosolic Ca^{2+} buffering

Chelation of intracellular Ca^{2+} in rabbit SANC by BAPTA (33, 46, 96), but not EGTA (46), applied intracellularly, markedly slowed or abolished spontaneous SANC beating. A strong negative chronotropic effect of EGTA, however, has been reported in guinea pig (SANC (97) and AV node cells (98)). That intracellular Ca^{2+} buffering blocks spontaneous AP generation is strong evidence that normal automaticity of these cells is tightly linked to intracellular Ca^{2+} dynamics. More recently Himeno et al. (99), however, reported patch clamp experiments and numerical modeling in guinea pig SANC which seem to refute the idea of a key role of Ca^{2+} dynamics in SANC function. The authors found that the spontaneous AP rate little changed when BAPTA, a Ca^{2+} chelator, was acutely infused via a patch pipette into SANC. The AP firing rate decreased, but only after several minutes of BAPTA infusion. They interpreted this result to indicate that while Ca^{2+} homeostasis is likely important (e.g. to support generation of cAMP by Ca^{2+}-activated ACs. Fig.1A), the Ca^{2+} dynamics, per se, (i.e. Ca^{2+} clock) are not important for spontaneous AP firing.

There is an alternative interpretation of this result (100). In short, the unexpected BAPTA effect can be explained on the basis of a small, artifactual patch seal leak current, a well-recognized artifact in whole-cell patch-clamp experiments that occurs when the membrane patch is ruptured. The occurrence of such leak currents immediately after patch rupture in the Himeno et al. experiments is evidenced by a clearly notable acute depolarization of MDP and an acute cell contracture (incomplete relaxation). The artifactual leak currents pose a serious problem during measurements of spontaneous AP firing because the DD is driven by a net current of a few pico-Amperes (25). In other words, small leak currents associated with seal electrical conductance likely shift the current balance of tiny DD currents, artificially increase the DD rate, and offset the true BAPTA effect that would, in the absence of the artifact, suppress the DD and prolong the cl. When a small leak current (~8 pA during DD

through a 6 GΩ seal resistance) is introduced into numerical model formulations (simulating experimental conditions of Himeno et al.), the coupled-clock ML-model does not fail, but continues to generate spontaneous APs when its Ca^{2+}-clock is acutely disabled (SR Ca^{2+} pumping rate set to zero), i.e. exactly as reported experimentally by Himeno et al. (99). The apparent long-term effects of BAPTA in Himeno et al. (99) study can be explained, in turn, by that in transition from perforated patch clamp to whole cell configuration, the perforating agent (amphotericin-B) quickly diffuses from patch pipette into cytosol and perforates the whole-cell membrane resulting in large artifactual leak currents and excitability loss.

Mini-summary

a. Intracellular Ca^{2+} buffering interferes with Ca^{2+} clock function that slows AP firing rate or halts automaticity.

b. Taking into account a delicate balance of ion currents (and high electrical resistance of SANC membrane) during DD, the results of whole-cell patch recordings should be treated with caution.

5.4 Beat-to-beat regulation of the cycle length by Ca^{2+} dynamics

While we have suggested an alternative explanation to the patch clamp results reported by Himeno at al. (99) (see previous section), the issues addressed by the authors are crucial in the context of beat-to-beat regulation of a coupled-clock pacemaker system and have prompted a new series of experimental and numerical modeling studies.

The role of Ca^{2+} in beat-to-beat regulation of SANC AP firing has been addressed further in a recent study by Yaniv et al. (101). When single isolated SANC are loaded with a caged Ca^{2+} buffer, NP-EGTA, the buffer markedly suppresses spontaneous diastolic LCRs and uncouples them from AP generation, causing AP firing to become markedly slower and dysrhythmic. When Ca^{2+} is acutely released from the caged compound by flash photolysis, intracellular Ca^{2+} dynamics are acutely restored and rhythmic APs resume immediately (at the same AP firing beat) to a normal AP firing rate. After a few rhythmic cycles, however, these effects of the flash wane as interference with Ca^{2+} dynamics (NP-EGTA dynamically buffers intracellular Ca^{2+}) by the caged buffer is reestablished. The acute, virtually instant, effect of the flash-induced Ca^{2+} release on the cycle length underscores importance of Ca^{2+} dynamics on the beat-to-beat basis.

Another recent study by Yaniv et al. (102) demonstrates that application of low concentrations of caffeine (2–4mM) to isolated single rabbit SA node cells under physiological conditions also acutely reduces their spontaneous AP cycle length.

Numerical simulations, using a modified ML “coupled-clock” model, faithfully reproduce the effects of cycle length prolongation and dys-rhythmic spontaneous beating produced by cytosolic Ca^{2+} buffering and also the acute cycle length reduction produced by both caffeine and flash-induced Ca^{2+} release (102). Three contemporary numerical models, Kurata et al. (66), Severi et al. (76) and the original ML model (10), fail to reproduce the experimental results (102). This most recent modification of ML model predicts that Ca^{2+} releases acutely change the cycle length via activation of the Na^{+}/Ca^{2+} exchanger current. Time-dependent

cycle length reductions after flash-induced Ca^{2+} releases ("memory" effect) are linked to changes in Ca^{2+} available for pumping into SR which, in turn, changes the SR Ca^{2+} load, diastolic Ca^{2+} releases and NCX current. These results support the idea that Ca^{2+} regulates cycle length in cardiac pacemaker cells on a beat-to-beat basis, and suggest a more realistic numerical mechanism of this regulation. Moreover, the model predicts that an increase in the sensitivity of RyR activation by lumenal SR Ca^{2+} (compared to submembrane) faithfully reproduces all changes in parameters of AP-induced Ca^{2+} transients measured experimentally in the low-caffeine experiments.

Finally, it was shown that while the entire LCR ensemble accelerates DD via activation of I_{NCX}, the intrinsic beat-to-beat variations in activation of individual stochastic LCRs generate the respective intrinsic noise in a non-linear DD component leading to cycle length variations; and this noise can be pharmacologically reduced or increased by respective perturbation of Ca^{2+} cycling in SANC (65). The beat-to-beat regulation of SANC AP cycle length by the fluctuating LCR ensemble has been recently directly demonstrated by measuring local Ca^{2+} signals by a high speed camera simultaneously with membrane potential recording (50). The study demonstrated that while the timing of each LCR occurrence during DD varies, the averaged period for all LCRs (i.e. the entire LCR ensemble) in a given cycle closely predicts the time of occurrence of the next AP, i.e. the AP cycle length. The crucial impact of the LCR ensemble on the fluctuations of AP cycle length had previously been demonstrated by numerical modeling (65). In this older, naive model, however, the LCRs, per se, were not predicted by the model, but rather described by an ensemble of sine functions directly mimicking characteristics of LCRs measured experimentally (as discussed in Section 4.1). Realistic numerical modeling of the intrinsic beat-to-beat variations of the AP cycle length requires inclusion of a theoretical mechanism of LCR generation in SANC based on local Ca^{2+} control mechanisms (Section 5.8).

Mini-summary

- **a.** Ca^{2+} regulates AP cycle length in SANC on a beat-to-beat basis.
- **b.** Intrinsic cycle length variability in single SANC is linked to beat-to-beat variations in the average period of individual LCRs each cycle.
- **c.** A new modification of ML model has been recently developed to reproduce new experimental data on beat-to-beat regulation using flash-induced and caffeine-induced Ca^{2+} releases.
- **d.** Future numerical modeling of beat-to-beat regulation ought to be based on local control mechanisms (for details see Section 5.8 below).

5.5. The problem of sodium regulation

Because the ML model considers dynamic variations of voltage and ion concentrations, it belongs to a so called "second-generation" of models (40). While models of this type describe complex and physiologically realistic interplay of electrophysiological and ionic mechanisms, some models have problems with 1) "degeneracy" i.e. the existence of a continuum of equilibrium points and 2) slow ion concentration drifts ((103–105), review (40)). For example, steady-state ion balance is achieved within hours of simulations in a

model of atrial cell AP by Kneller et al. (104)). A slow drift in Luo–Rudy dynamic model for ventricular cells was found to be due to the external stimulation current (103). While pacemaker cell modeling does not include external stimulation currents, a suggested practical solution to the problems of drift and degeneracy is to set the intracellular $[Na^+]$ and $[K^+]$ to constant values and treat them as independent model parameters (40, 106). Thus, intracellular $[Na^+]$ and $[K^+]$ were fixed to 10 mM and 140 mM, respectively, in Kurata et al. (107) and the ML model (10).

Fixing $[Na^+]$, on the other hand, obviously imposes a substantial limitation to the exploration of the pacemaker cell system, because the level of intracellular $[Na^+]$ is an important variable that determines functions of key molecules, e.g. the NCX and the electrogenic Na^+/K^+ pump. Experimental data on Na^+ regulation in SANC, however, is extremely limited (31, 108), preventing accurate modeling of $[Na^+]$ dynamics. For this reason a finding in a recent theoretical study of Kurata et al. (109) that I_f decreases the robustness of SANC pacemaking via I_f-dependent changes in intracellular $[Na^+]$, should be treated with caution. While a recent model by Severi et al. (76) describes Na^+ dynamics, their model could not keep Na^+ homeostasis upon intracellular Ca^{2+} buffering and, therefore, failed to reproduce negative chronotropic effect observed experimentally under these conditions (102).

Mini-summary

- **a.** While Na^+ regulation in SANC is an important part of cardiac pacemaker cell function, its present numerical modeling is likely unrealistic, due, in part, to a paucity of experimental measurements of Na^+ in pacemaker cells.
- **b.** Additional experimental and numerical model studies are required to clarify the role and the mechanisms of Na^+ regulation in SANC.

5.6. Energy consumption principle: issue of I_{NaK} matching $I_{b,Na}$

The energy consumption principle is yet another important issue (also related to Na^+ regulation discussed above) that had been raised by DiFrancesco in relation to considerations of the size of currents required for pacemaking (110). According to this principle "*all possible systems compatible with activity, the one which is most likely to be selected is the least energy consuming.*" In this regard, large background currents, such as $I_{b,Na}$, remaining within formulations of pacemaker cell models since 1960 (6), provide constant ion fluxes (i.e. Na^+ influx via $I_{b,Na}$) during all phases of the AP and basically shortcut the membrane. If such currents were present in a real SA node cell, the cell energy budget to retain ion (Na^+) homeostasis would be terribly high (44). Indeed, for example, in the Kurata et al. model (66), the magnitude of I_{NaK} (and therefore the magnitude of the related energy budget) was linked to the influx of Na^+ through $I_{b,Na}$ (and I_{st}) and efflux of K^+ through K^+ channels. Thus, presence of a large-scale $I_{b,Na}$ (alone, or in combination with I_{st}) in a model automatically imposes the presence of a respective, large-scale I_{NaK}.

DiFrancesco further argues that "*limiting, as with If, the inward current to the size and time-window strictly necessary to only generate the diastolic depolarization clearly helps reduce the energy consumption.*" We believe that this is also true for the component of I_{NCX} that is

activated by LCRs in the time window of DD. Furthermore, a broad parametric sensitivity analysis has recently demonstrated that in some SANC models, I_{NCX} can operate in the reverse mode during the AP (Fig.8A) and assist in extrusion of Na^+, resulting in less Na^+/K + ATPase activity to keep cell Na^+ balance (44). In this case the integral of Na^+ influx is substantially reduced compared to prior models (black bars in Fig.8B), and the energy budget is greatly improved (Fig.8C). While this type of model seems to be more realistic based on the energy consumption principle, it requires further experimental validation.

Mini-summary

a. The energy consumption principle is an important concept with respect to developing realistic pacemaker cell models.

b. Because background currents increase energy expenditure, their magnitude and existence should be carefully considered in numerical models in order to avoid unrealistically high energy budgets.

c. A large contribution of $I_{b,Na}$ in contemporary models contradicts the energy consumption principle.

d. In contrast to background currents, voltage activation of I_f and voltage- and LCR-activation of I_{NCX} (generating Na^+ influx) during DD occurs during a short time window at a relatively small energy cost.

e. Reverse mode NCX, extruding Na^+ during AP, might be an additional resource to save cell energy (as predicted by some numerical models). This possibility, however, needs an experimental validation.

5.7. Ion currents lacking molecular identity and selective blockers: $I_{b,Na}$ and I_{st}

As we discussed in section 3.1., H-H theory and its application to heart pacemaker cells by Noble in 1960 (6) inspired numerous voltage clamp studies which identified numerous ion currents in pacemaker cells (some of them listed in Table 1). All these currents were included in subsequent pacemaker cell numerical model updates (40). Therefore the present model formulations (reflecting the full history of ion current discoveries) become extremely complicated, featuring about a dozen of different ion currents. Some ion currents, however, still lack a molecular identity and selective blockers, despite the fact that they were identified in patch clamp recordings a long time ago. Thus, for future realistic modeling, it is critical to clarify if these currents are generated by unique, still unidentified molecules or by a combination of some known molecules (generating other currents). For example, both $I_{b,Na}$ and I_{st} are Na^+ currents. Given the lack of selective blockers, these currents (when experimentally recorded) could be generated, at least in part, by NCX. If so, then in the old detailed models this part of Na^+ flux is counted twice or thrice, i.e. by in I_{NCX}, I_{st}, and $I_{b,Na}$, resulting in overestimation of total Na^+ flux and, therefore, nonrealistic (worse than real) energy expenditure to keep Na^+ homeostasis in these models.

Given the paucity of $I_{b,Na}$ measurements reported in the literature, the magnitude or even the existence of $I_{b,Na}$ is clearly challenged by the molecular identity consideration, and also by the energy budget consideration (c.f. previous section). It has been speculated that a Na^+-H^+

mechanism contributes to the background current because it is reduced by amiloride (29). Another interesting idea is that background current is generated by a non-transported Na^+-Ca^{2+} leak of NCX (111). It can be also generated by a normal NCX operation in the forward mode: Indeed, a persistent component of inward I_{NCX} has been reported in guinea pig SANC (97) at the MDP and during the early DD. This I_{NCX} persistent component is also predicted by the ML model simulations (Fig.2, "I_{NCX} activation by hyperpolarization" and "I_{NCX} activation by Ca^{2+} transient"). A radical idea is that a background current does not exist in SANC, but is simply an artifact of the seal leak that always accompanies a whole-cell patch clamp recording (25).

A non-selective I_{st} (26) has many characteristics of I_{CaL}, e.g. it is sensitive to dihydropyridines and has a reversal potential close to 37 mV. However, I_{st} is activated at more negative potentials than I_{CaL} and achieves its peak at about −50 mV (112), i.e. exactly when LCRs begin to occur and activate I_{NCX} during DD. I_{st} exhibits other characteristics of I_{NCX}: it is mainly carried by Na^+, increased at lower extracellular [Ca^{2+}], but reduced at lower extracellular [Na^+] (26). Thus, it is possible that I_{st} reflects combined (direct and indirect) effects of I_{NCX} and I_{CaL}. In this case I_{st} sensitivity to dihydropyridines can be explained within the coupled-clock theory: a selective reduction of I_{CaL} reduces Ca^{2+} influx, the cell Ca^{2+} and SR Ca^{2+} loads, and hence reduces LCRs and LCR-induced I_{NCX}.

However, the issue with $I_{b,Na}$ and I_{st} representing phenomenological surrogates of other currents (I_{CaL}, I_{NCX}) cannot be resolved by numerical model simulations, per se, and probably requires a dedicated experimental study combined with numerical modeling. Indeed, any current representing a combination of fundamentally important currents would also seem to be extremely important in simulations (including autonomic modulation in case of I_{st} (113)); but this result would be obviously misleading and provide no guidance for emergent new technologies, such as genetically engineered biological pacemakers (discussed below) targeting specific molecules.

A recent pacemaker cell numerical model developed by Kharche et al. (114) was claimed to be "with molecular bases". This model, however, still includes formulations and substantial contributions of $I_{b,Na}$ and I_{st} having no molecular bases. Interpretations of numerical model simulations with contributions of these (and other) currents with no molecular identity can be misleading because their contributions will inevitably replace, in part, the contributions of other currents produced by known molecules. A recent large-scale parametric sensitivity analysis of numerical models of SANC based on a minimal set of sarcolemmal electrogenic proteins and an intracellular Ca^{2+} clock discovered a large cohort of models lacking $I_{b,Na}$ and I_{st} that can generate robust, flexible, and energy-efficient cardiac pacemaking (44). This study indicates that inclusion of $I_{b,Na}$ and I_{st} is not required for realistic (molecular based) modeling of pacemaker cell function.

Mini-summary

a. Some currents, such $I_{b,Na}$ and I_{st}, in formulations of contemporary numerical pacemaker cell models have no molecular identity.

b. The continued inclusion of these ion currents into pacemaker cell numerical models becomes problematic because their presence "steals" importance from the true molecular mechanisms of cardiac pacemaking.

c. Numerical models generating robust, flexible, and energy-efficient cardiac pacemaking can be constructed without $I_{b,Na}$ and I_{st} contributions (44).

5.8. Local Ca^{2+} control mechanisms

Within a traditional electrophysiological approach to cardiac cell pacemaker function (using the M-clock perspective), local activation of effector molecules, i.e. ion channels, do not matter, because a local electric charge change on the cell membrane associated with an opening of a channel (or a group of channels) becomes almost instantaneously spread over the entire cell membrane capacitor. The charge equilibrates for the whole cell length within ~20 microseconds estimated based on calculations of the propagation velocity of the electric charge disturbance using a cable equation (see Appendix in (54)). Thus from the "M-clock" perspective, approximation of the cell membrane as a single electric capacitor is well justified.

The situation with local signaling is fundamentally different with respect to Ca^{2+} dynamics. Ca^{2+} releases are generated locally and, in contrast to the membrane potential, the released Ca^{2+} does not propagate instantly across the length of the cell. Rather it diffuses relatively slowly and activates (recruit to fire) RyR via local CICR along the way, thus forming LCRs. The LCRs activate local NCX currents and local pumping (via SERCA). There is an entirely different and unexplored world of cardiac pacemaker mechanisms waiting to be discovered using a combination of powerful theoretical and experimental approaches that have been developed in classical studies of excitation-contraction coupling in cardiac muscle cells (review (115)), but previously thought to be hardly related to cardiac pacemaker mechanisms.

While the LCRs have been identified in pacemaker cells by confocal microscopy more than 10 years ago (35, 49), their theoretical formulations and numerical modeling lag behind. As the matter of fact, almost all numerical pacemaker cell models developed so far belong to so-called "common pool" models that simulate only total ("global") Ca^{2+} signals, but contain no terms that explore local Ca^{2+} control and RyR recruitment in SANC (i.e. LCRs). In short, Ca^{2+} signals (if any) in each cell compartment, e.g. cytosol, submembrane space, free (or network) SR, junctional SR, are described in common pool models by only one variable (Ca_i, Ca_{sub}, Ca_{nSR}, Ca_{jSR}, respectively, in Kurata et al. and the ML model).

A fundamental insufficiency of common pool models and crucial importance of local Ca^{2+} signaling in cardiac cells was demonstrated in a seminal report of local Ca^{2+} control theory (116). This theory explained graded CICR phenomenon via statistics of success and failure of an initiating event (such as an opening of LCCh) to recruit stochastic Ca^{2+} release units (CRUs) to fire. With respect to pacemaker cells, persisting roughly periodic LCRs observed in depolarized rabbit SANC are reproduced by a model of a locally distributed SR linked to submembrane space consisting of a two dimensional array of stochastic, diffusively coupled CRUs with fixed refractory period (117) (Fig.9). Because previous experimental studies

(118) showed that β-AR stimulation increases the rate of Ca^{2+} release through each CRU (dubbed I_{spark}), it is interesting to explore the link between LCRs and the I_{spark}. Numerical model simulations (117) show that increasing I_{spark} facilitates CICR and local recruitment of neighboring CRUs to fire more synchronously. These complex local interactions lead to a progression in simulated LCR size (from sparks to wavelets to global waves), LCR rhythmicity, and decrease of LCR period that parallels the changes observed experimentally with β-AR stimulation. The transition in LCR characteristics is steeply non-linear over a narrow range of I_{spark}, resembling a phase transition. Thus the (partial) periodicity and rate regulation of the "Ca^{2+} clock" in SANC are, at least in part, emergent properties of the diffusive coupling of an ensemble of interacting stochastic CRUs. The variation in LCR period and size with I_{spark} is sufficient to account for β-adrenergic regulation of SANC AP firing rate.

Although the aforementioned model simulations (117) provide new insights into LCR formation and β-AR stimulation of the local Ca^{2+} clock, they lack interactions with M-clock. A new, fully integrated model, featuring the local Ca^{2+} control approach with complete electrophysiological formulations (i.e. M-clock), has been recently developed (119) and applied to interpret results obtained in an incomplete knock-out (KO) NCX mouse model (120). SANC isolated from the incomplete KO mice exhibited no changes in AP firing rates, Ca^{2+} transient shapes, or ion current densities (other than I_{NCX}) measured under voltage clamp. However, the cells were insensitive to β-adrenergic receptor (β-AR) stimulation. Based on these and other results, Gao et al. (120) concluded that NCX expression is required for increasing sinus rates, but not for maintaining resting heart rate.

Numerical model simulations, however, demonstrate that local Ca^{2+} control mechanisms substantially contribute to I_{NCX} stabilization in SANC so that when the expression of NCX molecules is substantially reduced (to 20% of control, wild type), the diastolic I_{NCX} remains almost unchanged (Fig.10). Specifically, lower NCX expression facilitates local CICR and larger (diastolic) local Ca^{2+} releases (Fig.10A, right-hand panels) that stabilize diastolic I_{NCX} (Fig.10B). Further reduction of NCX expression results in arrhythmia and a cessation of automaticity (119), reproducing experimental findings in other (more complete) KO models (121, 122).

In addition to the important local NCX-RyR interactions, revealed by the new models, there are several further considerations as to why specific mechanisms are expected to be so different in the future local control models vs. present common pool models. Local [Ca^{2+}] in the vicinity of a Ca^{2+} spark or an LCR could be two orders of magnitude higher than average diastolic Ca^{2+} levels attained in common pool models. This difference has important consequences for approximation of SR Ca^{2+} pumping and release and also RyR-LCCh crosstalk in the models:

1) **The SR Ca^{2+} pumping** is more efficient in local control models. Indeed, the SR Ca^{2+} pumping rate is determined by a function of cytosolic [Ca^{2+}]. Because each LCR results in very high local Ca^{2+} concentrations, it fully activates Ca^{2+} pumping of the SR in its vicinity. On the other hand, in common pool models a diastolic Ca^{2+} release of a similar magnitude (e.g. an LCR) is spatially averaged over the entire compartment (i.e. pool, such as the

cytosol), and [Ca^{2+}] does not reach the high levels achieved in the local model. Therefore in a common pool model in response to a small total Ca^{2+} release of an LCR the SERCA operates in the region close to the foot of the sigmoid curve relating Ca^{2+} pumping rate to the [Ca^{2+}]. As a result only a relatively slow pumping rate is achieved in this case.

Additional numerical model simulations (119) show that the local Ca^{2+} control mechanism can ensure low (physiological) levels of diastolic Ca^{2+}, despite a substantial reduction in Ca^{2+} efflux capabilities (achieved mainly via NCX), e.g. in the incomplete NCX KO cells (120). In contrast, common pool models predict unrealistic high diastolic [Ca^{2+}] levels (119) which contradict the experimental measurements in these cells (120).

2) **The SR Ca^{2+} release** is also fundamentally different in local control models. A Ca^{2+} spark can effectively recruit neighboring CRUs to fire more Ca^{2+} sparks. Thus, LCRs are generated via propagating CICR that is described by stochastic recruitment of the CRUs. Common pool models do not describe this local Ca^{2+} diffusion-reaction paradigm. Their Ca^{2+} release is often described by a simple sigmoid (or power) function, relating global Ca^{2+} release flux to a global [Ca^{2+}] in the release pool (e.g. Ca_{sub} in Kurata et al. model (66)). Because any initiating Ca^{2+} release is instantaneously spread over the entire release pool in these models, it results in a relatively small change in the global [Ca^{2+}]. In this case CICR is small because Ca^{2+} release flux remains almost unchanged at the foot of the sigmoid (or power) function in response to the small change in [Ca^{2+}]. Whether or not the global release emerging from a multitude of wavelet-like LCRs can be reduced to a simple function of characteristics of interacting components (CRUs, buffers, diffusion coefficients, etc.) is not obvious and needs special theoretical considerations, similar to those in statistical physics.

3) **RyR-LCCh crosstalk** is another crucial interaction that can be realistically described only by local Ca^{2+} control mechanisms. One classical interaction happens during AP (similar to ventricular myocytes) when LCCh recruit RyR to generate Ca^{2+} transient. As we mentioned, these interactions are correctly described by local Ca^{2+} control theory developed by Stern (116). Also, a diastolic LCR (preceding an AP) can affect neighboring LCCh function via Ca^{2+} -dependent inactivation mechanism. Finally, threshold openings of LCCh can occur at membrane potentials (close to −45 mV) embracing the late DD phase and thereby facilitate local CICR, i.e. LCR generation, that, in turn, generate more local I_{NCX} and accelerate DD further, activating more LCCh openings, etc. This positive-feedback local process is analogous to an avalanche or a “rocket launch” and might have evolved in nature for a fail-safe generation of AP at the right time to ensure rhythmic pacemaker function.

There are several specific open problems that could be approached in the nearest future by the new local Ca^{2+} control models. The current model of LCR (117, 119) assumes a given restitution time for CRU during which it cannot fire a next release. Future studies ought to approach emergence of local Ca^{2+} clocking based on local SR Ca^{2+} pumping, refilling, and release mechanisms, predicting the restitution time, rather than taking it as an independent, phenomenological parameter of the model. A crucial importance of SR Ca^{2+} refilling kinetics for AP firing rate in SANC has been demonstrated in experimental studies utilizing direct measurements of local intra-SR Ca^{2+} signals (69). It is important to note that recent

studies of Ca^{2+} spark mechanisms (123) demonstrated that Ca^{2+} sparks can operate (activate and terminate) without a time dependent inactivation (never observed in studies of cardiac RyR channel gating in planar lipid bilayers). Thus, Ca^{2+} release restitution is not an inherent property of RyR molecules, but rather an emergent property of the system that includes complex interactions among local Ca^{2+} SR depletion-refilling, cytosolic Ca^{2+} depletion (via Ca^{2+} diffusion and SERCA pumping), and Ca^{2+}-dependent activation of RyR opening.

The first successful attempts to create such new models have been recently reported (124, 125). These new models have revealed a crucial importance of the spatial organization of the RyR and SERCA networks within SANC for pacemaker function. Specifically new simulations (124) demonstrated that the irregularity in RyR distribution in SANC is not a noise or imperfection, but rather a functional modality of the pacemaker cells that allows them to gradually engage CRUs to satisfy the chronotropic demand of the heart at a given condition.

The most recent SANC model simulates stochastic spontaneous diastolic Ca^{2+} release in 3 dimensions (125), based on explicit gating of individual Ca^{2+} channels (both RyR and LCCh), without assuming either a discrete sub-membrane compartment (used in many prior models (10, 66, 76, 117, 119)) or an inactivated state of the RyR. The model succeeded in reproducing propagating LCRs and realistic pacemaker rates only when RyR locations were assigned taking into account irregular, hierarchical distribution of RyR clusters observed in 3D confocal scan sections of immunofluorescence staining. The RyR spatial distribution was modelled as a variable network of RyR clusters, with small clusters intermediate between major ones, located immediately below the surface membrane. Interestingly, when the RyR sensitivity to Ca^{2+} is very high or NCX density is low, there is a paradoxical regime in which synchronization is lost, causing sympathetic stimulation to reduce rather than increase beating rate. This regime may be important for rhythm abnormalities caused by heart failure, RyR mutations, or pharmacological NCX blockade (126).

As mentioned above, LCR sizes undergo a phase-like transition with increasing of I_{spark} (i.e. Ca^{2+} release magnitude) in an agent-based model of stochastic recruitment of CRU to fire (117). How the interaction between the CRUs via CICR causes self-organization of Ca^{2+} spark clusters has recently been also studied in another agent-based model (of a mouse ventricular myocyte) (127). The statistics of the LCR sizes follow an exponential distribution when the coupling between CRUs is weak. As the interactions between CRUs strengthen, the LCR size distribution changes to a power-law distribution, which is indicative of criticality in complex nonlinear systems. The criticality underlies the formation and propagation of Ca^{2+} wavelets and waves resulting in whole-cell Ca^{2+} oscillations. While self-organized criticality describes (in statistical terms) numerous phenomena in nature from earthquakes and solar flares to fluctuations of stock market prices (128), the theory does not provide clean solutions as to how the macroscopic properties emerge from interactions of complex system components. Moreover, criticality was found in permeabilized ventricular myocytes with perpetuating Ca^{2+} releases of different sizes (127). During spontaneously AP firing by SANC, however, the Ca^{2+} release dynamics is further complicated by AP-induced Ca^{2+} release each cycle that would obviously prevent emergence of larger and longer lasting events, which are essentially required for criticality (Note, criticality is characterized by a

power law distribution of events on a broad time or space scale, usually reported on a log-log plot).

Mini-summary

a. Existing common pool models of SANC are incomplete: the amplitudes of Ca^{2+} dynamics can differ from those attained locally by two orders of magnitude. These naive models lack specific terms to describe true biophysical mechanisms of Ca^{2+} dynamics in SANC, such as local diffusion-reaction for the release, local efficient pumping and local NCX activation.

b. A new generation of model featuring local Ca^{2+} control will provide novel insights into cardiac pacemaker cell function.

c. The local control models can approach the current open problems, such as the existence of submembrane space, specific local interactions of RyR, SERCA, NCX and LCCh, underlying emergence and maintenance of local and global Ca^{2+} clocking, and robust and yet flexible cardiac pacemaker function.

d. The concepts of the phase transition (117) and self-organized criticality (127) can serve as general theoretical frameworks to approach emergence of a multitude of Ca^{2+} oscillatory signals in SANC at different scales of space and time. However insights from these theoretical concepts are presently limited to reductionist studies of isolated Ca^{2+} clock (i.e. in permeabilized or depolarized cells) and numerical models.

6. Modern numerical and theoretical approaches to explore cardiac pacemaker function

6.1. Parametric sensitivity analysis

Numerical modeling is utilized to interpret experimental data in order to gain further insights into the complexity of pacemaker cell function and ultimately to establish general pacemaker mechanisms. Achieving this goal, however, is complicated by the fact that the SA node is a highly heterogeneous structure with substantial cell-to-cell variations of functional expression of many key molecules. For example, in rabbit SANC the density of I_{CaL} varies by an order of magnitude (129) and I_f density varies 3 fold (13), with the density being smaller in SANC of smaller size. The classical approach in the pacemaker field, however, has been to develop and to report a numerical model with a unique set of model parameters (40) that ideally would describe present experimental results (average data) and hopefully embrace a general pacemaker mechanism to serve as a prototype of a “unified” or “typical” pacemaker cell. Reporting just a unique set of parameters, however, obviously uncovers neither the robustness of the model (and hence of the suggested mechanisms), nor realistic behavior of the SA node comprised of cells with their intrinsic large-scale variations (e.g. I_{CaL} and I_f).

A modern computational approach to address such problems and to gain broader insights into physiological function is to explore not just a single model of the system, but a large population of models (recently reviewed by Cummins et al. (130)). This approach is based

on ample computation power of modern computers and tests system behavior within all, or almost all, possible combinations of parameters measured experimentally, i.e. within thousands or even millions of individual models of different cell types. It has been used in particular by Marder et al. to generate large databases of model neurons (131, 132). A large variety of models of ventricular myocytes with different properties have been also successfully tested to identify the roles of particular model components on AP characteristics (133) and various cell behaviors, including responses to drugs (2).

The parameter-sensitivity approach in SANC modeling was initiated by Kurata et al. (66) and has been extended more recently for a coupled-clock SANC system (10, 44, 134). This approach holds promise for addressing cell-to-cell variability and for developing a more definitive understanding of the complex pacemaker cell functions. Figure 11 shows a simple example of such analysis of complex interplay of I_{CaL} and SR Ca^{2+} pumping in a population of 5,917 numerical models revealing parameter combinations yielding either rhythmic AP firing (color-coded areas) or pacemaker failure. This example actually shows the integrated operation of the M- and Ca^{2+} clocks: the border for rhythmic firing (the bifurcation yellow line) extends towards lower I_{CaL} conductance values when Ca^{2+} clock function enhances (as SR Ca^{2+} pumping enhances). And vice versa, without rhythmic ignition signals generated by Ca^{2+} clock, M-clock substantially slowed (vector c→j), became dysrhythmic (vector b→h), or ceased (vector a→g). This parametric analysis demonstrates the synergism of M- and Ca^{2+} clocks in generating robust and flexible pacemaking.

The multi-parameter sensitivity analysis can also illustrate the system response to a complex perturbation (e.g. moderate PKA inhibition) that affects both clocks and therefore is represented by a vector (b→d) in the parametric space. Thus, in general, this new approach permits identification of physiologically important ranges of parameter combinations to simulate experimental data and to learn how the system robustness and flexibility emerge from the complex interplay of molecules within the coupled-clock system. This approach can be further extended in future studies to provide insights into pathological behaviors, such as sick sinus syndrome or sinus tachycardia (130).

Mini-summary

- **a.** The sensitivity analysis within a large population of models is a modern trend in computational studies. It generates and explores model predictions for combinations of parameters by varying their specific values over a meaningful range, covering individual cell-to-cell variations, physiological (and pathophysiological) responses, and responses to drugs or genetic modifications.
- **b.** Population-based modeling can be used to explore the complex interplay of intracellular and cell membrane molecular components in SANC
- **c.** This approach has demonstrated that a synergism of coupled Ca^{2+} clocks and M-clocks confers robust and flexible pacemaker function (10)

6.2. The "Minimal Models" (or Occam's razor) approach to establish general pacemaker mechanisms and to guide engineering of future biological pacemakers

Another approach to establish general mechanisms of cardiac pacemaker function follows Occam's razor principle (the principle of parsimony) and tests whether essential, common properties of cardiac pacemaker cell function (i.e. robustness and flexibility) can be achieved with fewer (or with minimal number of) functional components, rather than with numerous components of the current detailed models. Such an approach, combined with a wide scale parametric sensitivity analysis described above, has been applied to delineate general pacemaker mechanisms in hundreds of thousands of numerical models, featuring combinations of only 4 or 5 key electrogenic molecules and a Ca^{2+} clock (44). The extended ranges of SR Ca^{2+} pumping (i.e. Ca^{2+} clock performance) and conductance of ion currents were sampled, yielding a large variety of parameter combination, i.e. specific model sets.

Each set's ability to simulate autonomic modulation of human heart rate in response to stimulation of cholinergic and β-AR receptors was tested. Only those models that include a Ca^{2+} clock (including the minimal 4-parameter model "I_{CaL}+I_{Kr}+I_{NCX}+Ca^{2+} clock") were able to reproduce the full range of autonomic modulation (44) (Fig.12A–C). Inclusion of I_f or I_{CaT} decreased the flexibility, but increased the robustness of the models (a relatively larger number of sets did not fail testing). The models comprised of components with clear molecular identity (i.e. lacking $I_{b,Na}$ & I_{st}) portray more realistic pacemaking: A smaller Na^+ influx is expected to demand less energy for Na^+ extrusion (as discussed in Section 5.6, see also Fig.8). The new large database of the reduced coupled-clock numerical models provide a conceptual basis for a general theory of robust, flexible, and energy-efficient pacemaking based on realistic components. This numerical tool can also help in designing biological pacemakers with desired properties using a minimal set of specific electrogenic molecules.

One specific insight, which has been validated experimentally, relates to I_f expression. A study in dogs (135) compared two types of bio-pacemakers with adenylyl cyclase (AC1 type) expression and combined expression of AC1 and I_f. This study showed that I_f is not required for bio-pacemaking, but the artificial increase in I_f results in a higher basal heart rate, i.e. very similar to results of the numerical model study (Fig.12D). A similar

Mini-summary

- **a.** Employing Occam's razor to explore the pacemaker system behaviors with minimal set of components can be helpful for establishing general pacemaker mechanisms.
- **b.** The results of such analyses can also aid in designing biological pacemakers that require minimum manipulations of specific molecular targets to acquire desired performance in terms of stable rhythm and AP firing rate range.

6.3. Bifurcation analysis

Finally, another powerful approach to study complex pacemaker cell function is stability and bifurcation analyses which were pioneered and developed by Kurata et al. (66, 134). These analyses establish equilibrium points (EP), at which the system is stationary (i.e., the oscillatory system fails to function), the periodic orbits (limit cycles, "LC"), and their

stability as functions of model parameters. The difference of this theoretical approach (i.e. strict bifurcation analysis based on the concepts of bifurcation theory) from simple numerical solutions (10, 44) (discussed above) is that it can be used for more systematic and complete evaluation of dynamical properties of nonlinear systems such as SANC. Bifurcation analyses can determine stable and unstable EPs (and LCs) and assess their stability more rapidly and accurately than simple numerical integration of differential equations, which can determine only stable EPs (and LCs) but not unstable EPs (or LCs) or how key parameters affect instability of EPs. Furthermore, strict bifurcation analyses can explore complex nonlinear systems with multi-stability (coexistence of multiple stable EPs and LCs), whereas simple numerical integrations often provide incomplete or inaccurate results (for a detailed comparisons see (136)). On the other hand, simple numerical integrations can evaluate temporal behaviors of SANC, such as transient and arrhythmic (chaotic) behaviors, which cannot be determined by the strict bifurcation analysis. Furthermore, future application of bifurcation theory to examine behaviors of local Ca^{2+} control models is not trivial and needs to be established.

The most recent study performed by Kurata et al. (134) using bifurcation analysis confirmed crucial importance of SR Ca^{2+} pumping, NCX function, and I_{CaL} activation for the coupled-clock system operation reported in previous studies using direct numerical integration (10). Their analysis also revealed that the ML model does not exhibit Ca^{2+} oscillations at any clamped voltage and requires further tuning to reproduce oscillatory local Ca^{2+} releases and total membrane current reported in experimental studies (47, 48).

Mini-summary

- **a.** Strict bifurcation analyses are a powerful theoretical method to explore the mechanisms of different behaviors of dynamical systems, such as SANC.
- **b.** This method does not substitute or exclude analyses using simple numerical integration. Both methods have pros and cons and complement each other.
- **c.** Bifurcation analyses have confirmed a crucial importance of Ca^{2+} cycling for normal SANC function.

7. Summary and future directions

We have summarized the present state of numerical modeling approaches to cardiac pacemaking as a complex phenomenon that include integrated function of intracellular and cell membrane proteins. Mini-summaries after each section provide postulates and helpful statements to guide the future development of this research area. In short, we believe that the time of presenting insights from only a single set of parameters has passed. Rather, numerical modeling of pacemaker cells should explore the pacemaker cell system using sensitivity analyses in large- scale model populations and bifurcation analyses providing robust and ubiquitous insights. These new powerful approaches become possible due to easily available increased computing power. Studies, in which pacemaker cell function is reduced to only essential components (“Occam’s razor” approach), can also help establish general pacemaker mechanisms, because in this case, basically all possible individual models can be examined using the population-based approach. This approach can also aid in

designing biological pacemakers that require minimum manipulations of specific molecular targets to acquire desired performance in terms of stable rhythm and AP firing rate range.

We believe that the time of describing cardiac pacemaker cell essentially as a membrane voltage oscillator (via an interplay of H-H kinetics) has also passed. Numerous experimental studies validated by extensive numerical modeling over the last decade have established that pacemaker cell function cannot be reduced to functions of only sarcolemmal ion channels; rather, it is generated by a complex system of dynamically interacting components residing in cell membrane and inside the cells. In this critical review we have tried to approach existing paradoxes and controversies based on this ground.

Important future advances of the pacemaker cell modeling will include (a) more quantitative localization data describing nanoscale relations between RyR clusters, LCChs, NCX, and SERCA; (b) measurements of local SR Ca^{2+} refilling ("blink" kinetics) and/or restitution of sparks and LCRs, analogous to experiments that have been performed in ventricular cells, (c) better measurements of mitochondrial Ca^{2+} uptake and extrusion specifically in the SA node, (d) integration of biochemical pathways (especially linked to local cAMP production and protein phosphorylation), (e) and molecule-based modeling (i.e. limited to components with clear molecular identity).

While our review is focused on the cellular mechanisms of cardiac impulse initiation, the pacemaker function of the heart is determined by further complex integration of the cell signals within SA node tissue that include both pacemaker and non-pacemaker cells (e.g. fibroblasts, neurons, etc. The interested reader is referred to the most recent achievements in the numerical modeling in this exciting area of research (137, 138), including pathological aspects of SA node function (139, 140).

Acknowledgments

This research was supported by the Intramural Research Program of the National Institutes of Health, National Institute on Aging.

Anna V. Maltsev is a consultant of Pace Biologics, LLC, USA. Victor A. Maltsev and Edward G. Lakatta are co-inventors in the U.S. Provisional Patent Application No. 61/180,49 of 2009: “Engineered Biological Pacemakers”.

References

1. Noble D. Computational models of the heart and their use in assessing the actions of drugs. J Pharmacol Sci. 2008; 107:107–117. [PubMed: 18566519]
2. Sarkar AX, Sobie EA. Quantification of repolarization reserve to understand interpatient variability in the response to proarrhythmic drugs: a computational analysis. Heart Rhythm. 2011; 8:1749–1755. [PubMed: 21699863]
3. Noble D. Modelling the heart: insights, failures and progress. Bioessays. 2002; 24:1155–1163. [PubMed: 12447980]
4. Maltsev VA, Vinogradova TM, Lakatta EG. The emergence of a general theory of the initiation and strength of the heartbeat. J Pharmacol Sci. 2006; 100:338–369. [PubMed: 16799255]
5. Bozler E. Tonus changes in cardiac muscle and their significance for the initiation of impulses. Am J Physiol. 1943; 139:477–480.
6. Noble D. Cardiac action and pacemaker potentials based on the Hodgkin-Huxley equations. Nature. 1960; 188:495–497.

7. Fabiato A, Fabiato F. Excitation-contraction coupling of isolated cardiac fibers with disrupted or closed sarcolemmas. Calcium-dependent cyclic and tonic contractions. Circ Res. 1972; 31:293–307. [PubMed: 4341466]
8. Tsien RW, Kass RS, Weingart R. Cellular and subcellular mechanisms of cardiac pacemaker oscillations. J Exp Biol. 1979; 81:205–215. [PubMed: 512578]
9. Rubenstein DS, Lipsius SL. Mechanisms of automaticity in subsidiary pacemakers from cat right atrium. Circ Res. 1989; 64:648–657. [PubMed: 2467760]
10. Maltsev VA, Lakatta EG. Synergism of coupled subsarcolemmal Ca^{2+} clocks and sarcolemmal voltage clocks confers robust and flexible pacemaker function in a novel pacemaker cell model. Am J Physiol Heart Circ Physiol. 2009; 296:H594–H615. [PubMed: 19136600]
11. Lakatta EG, Maltsev VA, Vinogradova TM. A coupled SYSTEM of intracellular Ca^{2+} clocks and surface membrane voltage clocks controls the timekeeping mechanism of the heart's pacemaker. Circ Res. 2010; 106:659–673. [PubMed: 20203315]
12. Muramatsu H, Zou AR, Berkowitz GA, Nathan RD. Characterization of a TTX-sensitive Na+ current in pacemaker cells isolated from rabbit sinoatrial node. Am J Physiol. 1996; 270:H2108–H2119. [PubMed: 8764263]
13. Honjo H, Boyett MR, Kodama I, Toyama J. Correlation between electrical activity and the size of rabbit sino-atrial node cells. J Physiol. 1996; 496(Pt 3):795–808. [PubMed: 8930845]
14. Hagiwara N, Irisawa H, Kameyama M. Contribution of two types of calcium currents to the pacemaker potentials of rabbit sino-atrial node cells. J Physiol. 1988; 395:233–253. [PubMed: 2457676]
15. Nilius B. Possible functional significance of a novel type of cardiac Ca channel. Biomed Biochim Acta. 1986; 45:K37–K45. [PubMed: 2430559]
16. Tanaka H, Komikado C, Namekata I, Nakamura H, Suzuki M, Tsuneoka Y, et al. Species difference in the contribution of T-type calcium current to cardiac pacemaking as revealed by r(−)-efonidipine. J Pharmacol Sci. 2008; 107:99–102. [PubMed: 18460822]
17. Boyett MR, Honjo H, Yamamoto M, Nikmaram MR, Niwa R, Kodama I. Regional differences in effects of 4-aminopyridine within the sinoatrial node. Am J Physiol. 1998; 275:H1158–H1168. [PubMed: 9746462]
18. Honjo H, Lei M, Boyett MR, Kodama I. Heterogeneity of 4-aminopyridine-sensitive current in rabbit sinoatrial node cells. Am J Physiol. 1999; 276:H1295–H1304. [PubMed: 10199855]
19. Lei M, Honjo H, Kodama I, Boyett MR. Characterisation of the transient outward K+ current in rabbit sinoatrial node cells. Cardiovasc Res. 2000; 46:433–441. [PubMed: 10912454]
20. Ito H, Ono K. A rapidly activating delayed rectifier K+ channel in rabbit sinoatrial node cells. Am J Physiol. 1995; 269:H443–H452. [PubMed: 7653608]
21. Lei M, Brown HF. Two components of the delayed rectifier potassium current IK, in rabbit sino-atrial node cells. Exp Physiol. 1996; 81:725–741. [PubMed: 8889473]
22. Satoh H. Sino-atrial nodal cells of mammalian hearts: ionic currents and gene expression of pacemaker ionic channels. J Smooth Muscle Res. 2003; 39:175–193. [PubMed: 14695028]
23. Yanagihara K, Irisawa H. Inward current activated during hyperpolarization in the rabbit sinoatrial node cell. Pflugers Arch. 1980; 385:11–19. [PubMed: 7191093]
24. Maylie J, Morad M, Weiss J. A study of pace-maker potential in rabbit sino-atrial node: measurement of potassium activity under voltage-clamp conditions. J Physiol. 1981; 311:161–178. [PubMed: 7264968]
25. DiFrancesco D. The contribution of the 'pacemaker' current (i_f) to generation of spontaneous activity in rabbit sino-atrial node myocytes. J Physiol. 1991; 434:23–40. [PubMed: 2023118]
26. Guo J, Ono K, Noma A. A sustained inward current activated at the diastolic potential range in rabbit sino-atrial node cells. J Physiol. 1995; 483(Pt 1):1–13. [PubMed: 7776225]
27. Reuveny E, Slesinger PA, Inglese J, Morales JM, Iniguez-Lluhi JA, Lefkowitz RJ, et al. Activation of the cloned muscarinic potassium channel by G protein beta gamma subunits. Nature. 1994; 370:143–146. [PubMed: 8022483]
28. Ju YK, Chu Y, Chaulet H, Lai D, Gervasio OL, Graham RM, et al. Store-operated Ca^{2+} influx and expression of TRPC genes in mouse sinoatrial node. Circ Res. 2007; 100:1605–1614. [PubMed: 17478725]

29. Hagiwara N, Irisawa H, Kasanuki H, Hosoda S. Background current in sino-atrial node cells of the rabbit heart. J Physiol. 1992; 448:53–72. [PubMed: 1317444]
30. Noma A, Irisawa H. Contribution of an electrogenic sodium pump to the membrane potential in rabbit sinoatrial node cells. Pflugers Arch. 1975; 358:289–301. [PubMed: 1172612]
31. Sakai R, Hagiwara N, Matsuda N, Kassanuki H, Hosoda S. Sodium--potassium pump current in rabbit sino-atrial node cells. J Physiol. 1996; 490(Pt 1):51–62. [PubMed: 8745278]
32. Rigg L, Terrar DA. Possible role of calcium release from the sarcoplasmic reticulum in pacemaking in guinea-pig sino-atrial node. Exp Physiol. 1996; 81:877–880. [PubMed: 8889484]
33. Li J, Qu J, Nathan RD. Ionic basis of ryanodine's negative chronotropic effect on pacemaker cells isolated from the sinoatrial node. Am J Physiol. 1997; 273:H2481–H2489. [PubMed: 9374788]
34. Satoh H. Electrophysiological actions of ryanodine on single rabbit sinoatrial nodal cells. Gen Pharmacol. 1997; 28:31–38. [PubMed: 9112074]
35. Bogdanov KY, Vinogradova TM, Lakatta EG. Sinoatrial nodal cell ryanodine receptor and Na^+ - Ca^{2+} exchanger: molecular partners in pacemaker regulation. Circ Res. 2001; 88:1254–1258. [PubMed: 11420301]
36. Hagiwara N, Irisawa H. Na-Ca exchange current in sinoatrial node cell of rabbit. Circulation. 1988; (Suppl 78):490a. (Abstract).
37. Verkerk AO, Wilders R, Zegers JG, van Borren MM, Ravesloot JH, Verheijck EE. Ca^{2+} - activated Cl^- current in rabbit sinoatrial node cells. J Physiol. 2002; 540:105–117. [PubMed: 11927673]
38. Noma A. Ionic mechanisms of the cardiac pacemaker potential. Jpn Heart J. 1996; 37:673–682. [PubMed: 8973380]
39. Mangoni ME, Nargeot J. Genesis and regulation of the heart automaticity. Physiol Rev. 2008; 88:919–982. [PubMed: 18626064]
40. Wilders R. Computer modelling of the sinoatrial node. Med Biol Eng Comput. 2007; 45:189–207. [PubMed: 17115219]
41. DiFrancesco D, Ojeda C. Properties of the current if in the sino-atrial node of the rabbit compared with those of the current iK, in Purkinje fibres. J Physiol. 1980; 308:353–367. [PubMed: 6262501]
42. Verkerk AO, Wilders R. Hyperpolarization-Activated Current, I f, in Mathematical Models of Rabbit Sinoatrial Node Pacemaker Cells. Biomed Res Int. 2013; 2013:872454. [PubMed: 23936852]
43. Maltsev VA, Lakatta EG. A novel quantitative explanation for autonomic modulation of cardiac pacemaker cell automaticity via a dynamic system of sarcolemmal and intracellular proteins. Am J Physiol Heart Circ Physiol. 2010; 298:H2010–H2023. [PubMed: 20228256]
44. Maltsev VA, Lakatta EG. Numerical models based on a minimal set of sarcolemmal electrogenic proteins and an intracellular Ca clock generate robust, flexible, and energy-efficient cardiac pacemaking. J Mol Cell Cardiol. 2013; 59:181–195. [PubMed: 23507256]
45. Ju YK, Allen DG. Intracellular calcium and Na^+-Ca^{2+} exchange current in isolated toad pacemaker cells. J Physiol. 1998; 508(Pt 1):153–166. [PubMed: 9490832]
46. Vinogradova TM, Zhou YY, Bogdanov KY, Yang D, Kuschel M, Cheng H, et al. Sinoatrial node pacemaker activity requires Ca^{2+}/calmodulin-dependent protein kinase II activation. Circ Res. 2000; 87:760–767. [PubMed: 11055979]
47. Vinogradova TM, Lyashkov AE, Zhu W, Ruknudin AM, Sirenko S, Yang D, et al. High basal protein kinase A-dependent phosphorylation drives rhythmic internal Ca^{2+} store oscillations and spontaneous beating of cardiac pacemaker cells. Circ Res. 2006; 98:505–514. [PubMed: 16424365]
48. Vinogradova TM, Zhou YY, Maltsev V, Lyashkov A, Stern M, Lakatta EG. Rhythmic ryanodine receptor Ca^{2+} releases during diastolic depolarization of sinoatrial pacemaker cells do not require membrane depolarization. Circ Res. 2004; 94:802–809. [PubMed: 14963011]
49. Huser J, Blatter LA, Lipsius SL. Intracellular Ca^{2+} release contributes to automaticity in cat atrial pacemaker cells. J Physiol. 2000; 524(Pt 2):415–422. [PubMed: 10766922]
50. Monfredi O, Maltseva LA, Spurgeon HA, Boyett MR, Lakatta EG, Maltsev VA. Beat-to-beat variation in periodicity of local calcium releases contributes to intrinsic variations of spontaneous

cycle length in isolated single sinoatrial node cells. PLoS One. 2013; 8:e67247. [PubMed: 23826247]

51. Rigg L, Heath BM, Cui Y, Terrar DA. Localisation and functional significance of ryanodine receptors during beta-adrenoceptor stimulation in the guinea-pig sino-atrial node. Cardiovasc Res. 2000; 48:254–264. [PubMed: 11054472]
52. Ju YK, Allen DG. The distribution of calcium in toad cardiac pacemaker cells during spontaneous firing. Pflugers Arch. 2000; 441:219–227. [PubMed: 11211106]
53. Lakatta EG, Maltsev VA, Bogdanov KY, Stern MD, Vinogradova TM. Cyclic variation of intracellular calcium: a critical factor for cardiac pacemaker cell dominance. Circ Res. 2003; 92:e45–e50. [PubMed: 12595348]
54. Maltsev VA, Vinogradova TM, Bogdanov KY, Lakatta EG, Stern MD. Diastolic calcium release controls the beating rate of rabbit sinoatrial node cells: numerical modeling of the coupling process. Biophys J. 2004; 86:2596–2605. [PubMed: 15041695]
55. van Borren MM, Verkerk AO, Wilders R, Hajji N, Zegers JG, Bourier J, et al. Effects of muscarinic receptor stimulation on Ca^{2+} transient, cAMP production and pacemaker frequency of rabbit sinoatrial node cells. Basic Res Cardiol. 2010; 105:73–87. [PubMed: 19639379]
56. Joung B, Tang L, Maruyama M, Han S, Chen Z, Stucky M, et al. Intracellular calcium dynamics and acceleration of sinus rhythm by beta-adrenergic stimulation. Circulation. 2009; 119:788–796. [PubMed: 19188501]
57. Wu Y, Gao Z, Chen B, Koval OM, Singh MV, Guan X, et al. Calmodulin kinase II is required for fight or flight sinoatrial node physiology. Proc Natl Acad Sci U S A. 2009; 106:5972–5977. [PubMed: 19276108]
58. Lakatta EG, Vinogradova T, Lyashkov A, Sirenko S, Zhu W, Ruknudin A, et al. The integration of spontaneous intracellular Ca^{2+} cycling and surface membrane ion channel activation entrains normal automaticity in cells of the heart's pacemaker. Ann N Y Acad Sci. 2006; 1080:178–206. [PubMed: 17132784]
59. Sirenko S, Maltsev VA, Maltseva LA, Yang D, Lukyanenko Y, Vinogradova TM, et al. Sarcoplasmic reticulum Ca cycling protein phosphorylation in a physiologic Ca milieu unleashes a high-power, rhythmic Ca clock in ventricular myocytes: Relevance to arrhythmias and biopacemaker design. J Mol Cell Cardiol. 2014; 66C:106–115. [PubMed: 24274954]
60. Willoughby D, Cooper DM. Organization and Ca^{2+} regulation of adenylyl cyclases in cAMP microdomains. Physiol Rev. 2007; 87:965–1010. [PubMed: 17615394]
61. Mattick P, Parrington J, Odia E, Simpson A, Collins T, Terrar D. Ca^{2+}-stimulated adenylyl cyclase isoform AC1 is preferentially expressed in guinea-pig sino-atrial node cells and modulates the I_f pacemaker current. J Physiol. 2007; 582:1195–1203. [PubMed: 17540702]
62. Younes A, Lyashkov AE, Graham D, Sheydina A, Volkova MV, Mitsak M, et al. Ca^{2+} -stimulated basal adenylyl cyclase activity localization in membrane lipid microdomains of cardiac sinoatrial nodal pacemaker cells. J Biol Chem. 2008; 283:14461–14468. [PubMed: 18356168]
63. Vinogradova TM, Sirenko S, Lyashkov AE, Younes A, Li Y, Zhu W, et al. Constitutive phosphodiesterase activity restricts spontaneous beating rate of cardiac pacemaker cells by suppressing local Ca^{2+} releases. Circ Res. 2008; 102:761–769. [PubMed: 18276917]
64. Zahanich I, Li Y, Lyashkov AE, Lukyanenko YO, Vinogradova TM, Younes A, et al. Protein phosphatase 1 regulates normal automaticity of the heart's pacemaker node cells by site-specific modulation of phospholamban phosphorylation that regulates spontaneous subsarcolemmal local Ca^{2+} releases. Circulation. 2010; 122:A21546. (Abstract).
65. Bogdanov KY, Maltsev VA, Vinogradova TM, Lyashkov AE, Spurgeon HA, Stern MD, et al. Membrane potential fluctuations resulting from submembrane Ca^{2+} releases in rabbit sinoatrial nodal cells impart an exponential phase to the late diastolic depolarization that controls their chronotropic state. Circ Res. 2006; 99:979–987. [PubMed: 17008599]
66. Kurata Y, Hisatome I, Imanishi S, Shibamoto T. Dynamical description of sinoatrial node pacemaking: improved mathematical model for primary pacemaker cell. Am J Physiol. 2002; 283:H2074–H2101.
67. Shannon TR, Wang F, Puglisi J, Weber C, Bers DM. A mathematical treatment of integrated Ca dynamics within the ventricular myocyte. Biophys J. 2004; 87:3351–3371. [PubMed: 15347581]

68. Imtiaz MS, von der Weid PY, Laver DR, van Helden DF. SR Ca^{2+} store refill--a key factor in cardiac pacemaking. J Mol Cell Cardiol. 2010; 49:412–426. [PubMed: 20353793]
69. Vinogradova TM, Brochet DX, Sirenko S, Li Y, Spurgeon H, Lakatta EG. Sarcoplasmic reticulum Ca^{2+} pumping kinetics regulates timing of local Ca^{2+} releases and spontaneous beating rate of rabbit sinoatrial node pacemaker cells. Circ Res. 2010; 107:767–775. [PubMed: 20651285]
70. Yaniv Y, Maltsev VA, Ziman BD, Spurgeon HA, Lakatta EG. The "Funny" Current (I_f) Inhibition by Ivabradine at Membrane Potentials Encompassing Spontaneous Depolarization in Pacemaker Cells. Molecules. 2012; 17:8241–8254. [PubMed: 22777191]
71. Yaniv Y, Sirenko S, Ziman BD, Spurgeon HA, Maltsev VA, Lakatta EG. New evidence for coupled clock regulation of the normal automaticity of sinoatrial nodal pacemaker cells: Bradycardic effects of ivabradine are linked to suppression of intracellular Ca cycling. J Mol Cell Cardiol. 2013; 62C:80–89. [PubMed: 23651631]
72. Bois P, Bescond J, Renaudon B, Lenfant J. Mode of action of bradycardic agent, S 16257, on ionic currents of rabbit sinoatrial node cells. Br J Pharmacol. 1996; 118:1051–1057. [PubMed: 8799581]
73. Cappato R, Castelvecchio S, Ricci C, Bianco E, Vitali-Serdoz L, Gnecchi-Ruscone T, et al. Clinical efficacy of ivabradine in patients with inappropriate sinus tachycardia: a prospective, randomized, placebo-controlled, double-blind, crossover evaluation. J Am Coll Cardiol. 2012; 60:1323–1329. [PubMed: 22981555]
74. Yaniv Y, Spurgeon HA, Lyashkov AE, Yang D, Ziman BD, Maltsev VA, et al. Crosstalk between Mitochondrial and Sarcoplasmic Reticulum Ca^{2+} Cycling Modulates Cardiac Pacemaker Cell Automaticity. PLoS One. 2012; 7:e37582. [PubMed: 22666369]
75. Yaniv Y, Lakatta EG. Pacemaker gene mutations, bradycardia, arrhythmias and the coupled clock theory. Journal of Cardiovascular Electrophysiology. 2013; 24:E28–E29. [PubMed: 24015891]
76. Severi S, Fantini M, Charawi LA, DiFrancesco D. An updated computational model of rabbit sinoatrial action potential to investigate the mechanisms of heart rate modulation. J Physiol. 2012; 590:4483–4499. [PubMed: 22711956]
77. Demir SS, Clark JW, Giles WR. Parasympathetic modulation of sinoatrial node pacemaker activity in rabbit heart: a unifying model. Am J Physiol. 1999; 276:H2221–H2244. [PubMed: 10362707]
78. Lyashkov AE, Vinogradova TM, Zahanich I, Li Y, Younes A, Nuss HB, et al. Cholinergic receptor signaling modulates spontaneous firing of sinoatrial nodal cells via integrated effects on PKA-dependent Ca^{2+} cycling and I_{KACh}. Am J Physiol Heart Circ Physiol. 2009; 297:H949–H959. [PubMed: 19542482]
79. Dokos S, Celler B, Lovell N. Ion currents underlying sinoatrial node pacemaker activity: a new single cell mathematical model. J Theor Biol. 1996; 181:245–272. [PubMed: 8869126]
80. Zhang H, Holden AV, Kodama I, Honjo H, Lei M, Varghese T, et al. Mathematical models of action potentials in the periphery and center of the rabbit sinoatrial node. Am J Physiol. 2000; 279:H397–H421.
81. Yaniv Y, Ganesan A, Yang D, Ziman BD, Zhang J, Lakatta EG. Experimental and in silico studies of the kinetics and magnitude of PKA activation in live sinoatrial node pacemaker cell. J Mol Cell Cardiol. 2013 (Abstract).
82. Yaniv Y, Juhaszova M, Lyashkov AE, Spurgeon HA, Sollott SJ, Lakatta EG. Ca^{2+}-regulated-cAMP/PKA signaling in cardiac pacemaker cells links ATP supply to demand. J Mol Cell Cardiol. 2011; 51:740–748. [PubMed: 21835182]
83. Yaniv Y, Spurgeon HA, Ziman BD, Lyashkov AE, Lakatta EG. Mechanisms that match ATP supply to demand in cardiac pacemaker cells during high ATP demand. Am J Physiol Heart Circ Physiol. 2013; 304:H1428–H1438. [PubMed: 23604710]
84. De Stefani D, Raffaello A, Teardo E, Szabo I, Rizzuto R. A forty-kilodalton protein of the inner membrane is the mitochondrial calcium uniporter. Nature. 2011; 476:336–340. [PubMed: 21685888]
85. Palty R, Silverman WF, Hershfinkel M, Caporale T, Sensi SL, Parnis J, et al. NCLX is an essential component of mitochondrial Na^+/Ca^{2+} exchange. Proc Natl Acad Sci U S A. 2009; 107:436–441. [PubMed: 20018762]

86. Yaniv Y, Juhaszova M, Sollott SJ. Age-related changes of myocardial ATP supply and demand mechanisms. Trends Endocrinol Metab. 2013; 24:495–505. [PubMed: 23845538]
87. Yaniv Y, Juhaszova M, Nuss HB, Wang S, Zorov DB, Lakatta EG, et al. Matching ATP supply and demand in mammalian heart: in vivo, in vitro, and in silico perspectives. Ann N Y Acad Sci. 2010; 1188:133–142. [PubMed: 20201896]
88. Yaniv Y, Spurgeon HA, Lyashkov AE, Yang D, Ziman BD, Maltsev VA, et al. cAMP/PKA-dependent phosphorylation signaling controls both pacemaker cell rate and energetics: experimental evidence and in silco testing. Heart Rhythm. 2013; 10:S53. (Abstract).
89. Noble D. A modification of the Hodgkin-Huxley equations applicable to Purkinje fibre action and pace-maker potentials. J Physiol. 1962; 160:317–352. [PubMed: 14480151]
90. McAllister RE, Noble D, Tsien RW. Reconstruction of the electrical activity of cardiac Purkinje fibres. J Physiol. 1975; 251:1–59. [PubMed: 1185607]
91. Noble D, Noble SJ. A model of sino-atrial node electrical activity based on a modification of the DiFrancesco-Noble (1984) equations. Proc R Soc Lond B Biol Sci. 1984; 222:295–304. [PubMed: 6149553]
92. Beeler GW, Reuter H. Reconstruction of the action potential of ventricular myocardial fibres. J Physiol. 1977; 268:177–210. [PubMed: 874889]
93. DiFrancesco D, Noble D. A model of cardiac electrical activity incorporating ionic pumps and concentration changes. Philos Trans R Soc Lond B Biol Sci. 1985; 307:353–398. [PubMed: 2578676]
94. Noble D, Noble PJ, Fink M. Competing oscillators in cardiac pacemaking: historical background. Circ Res. 2010; 106:1791–1797. [PubMed: 20576941]
95. Brown HF, Kimura J, Noble D, Noble SJ, Taupignon A. The slow inward current, isi, in the rabbit sino-atrial node investigated by voltage clamp and computer simulation. Proc R Soc Lond B Biol Sci. 1984; 222:305–328. [PubMed: 6149554]
96. Lyashkov AE, Juhaszova M, Dobrzynski H, Vinogradova TM, Maltsev VA, Juhasz O, et al. Calcium cycling protein density and functional importance to automaticity of isolated sinoatrial nodal cells are independent of cell size. Circ Res. 2007; 100:1723–1731. [PubMed: 17525366]
97. Sanders L, Rakovic S, Lowe M, Mattick PA, Terrar DA. Fundamental importance of Na^+-Ca^{2+} exchange for the pacemaking mechanism in guinea-pig sino-atrial node. J Physiol. 2006; 571:639–649. [PubMed: 16423859]
98. Hancox JC, Levi AJ, Brooksby P. Intracellular calcium transients recorded with Fura-2 in spontaneously active myocytes isolated from the atrioventricular node of the rabbit heart. Proc Biol Sci. 1994; 255:99–105. [PubMed: 8165231]
99. Himeno Y, Toyoda F, Satoh H, Amano A, Cha CY, Matsuura H, et al. Minor contribution of cytosolic Ca^{2+} transients to the pacemaker rhythm in guinea pig sinoatrial node cells. Am J Physiol Heart Circ Physiol. 2011; 300:H251–H261. [PubMed: 20952667]
100. Maltsev VA, Vinogradova TM, Stern MD, Lakatta EG. Validating the requirement for beat-to-beat coupling of the Ca clock and M clock in pacemaker cell normal automaticity. Am J Physiol Heart Circ Physiol. 2011; 300:H2323–H2324. [PubMed: 21632980]
101. Yaniv Y, Maltsev VA, Escobar AL, Spurgeon HA, Ziman BD, Stern MD, et al. Beat-to-beat Ca^{2+}-dependent regulation of sinoatrial nodal pacemaker cell rate and rhythm. J Mol Cell Cardiol. 2011; 51:902–905. [PubMed: 21963899]
102. Yaniv Y, Stern MD, Lakatta EG, Maltsev VA. Mechanisms of beat-to-beat regulation of cardiac pacemaker cell function by Ca^{2+} cycling dynamics. Biophys J. 2013; 105:1551–1561. [PubMed: 24094396]
103. Hund TJ, Kucera JP, Otani NF, Rudy Y. Ionic charge conservation and long-term steady state in the Luo-Rudy dynamic cell model. Biophys J. 2001; 81:3324–3331. [PubMed: 11720995]
104. Kneller J, Ramirez RJ, Chartier D, Courtemanche M, Nattel S. Time-dependent transients in an ionically based mathematical model of the canine atrial action potential. Am J Physiol Heart Circ Physiol. 2002; 282:H1437–H1451. [PubMed: 11893581]
105. Krogh-Madsen T, Schaffer P, Skriver AD, Taylor LK, Pelzmann B, Koidl B, et al. An ionic model for rhythmic activity in small clusters of embryonic chick ventricular cells. Am J Physiol Heart Circ Physiol. 2005; 289:H398–H413. [PubMed: 15708964]

106. Guan S, Lu Q, Huang K. A discussion about the DiFrancesco-Noble model. J Theor Biol. 1997; 189:27–32. [PubMed: 9398500]

107. Kurata Y, Hisatome I, Imanishi S, Shibamoto T. Roles of L-type Ca^{2+} and delayed-rectifier K^{+} currents in sinoatrial node pacemaking: insights from stability and bifurcation analyses of a mathematical model. Am J Physiol Heart Circ Physiol. 2003; 285:H2804–H2819. [PubMed: 12919936]

108. Choi HS, Wang DY, Noble D, Lee CO. Effect of isoprenaline, carbachol, and Cs+ on Na+ activity and pacemaker potential in rabbit SA node cells. Am J Physiol. 1999; 276:H205–H214. [PubMed: 9887034]

109. Kurata Y, Hisatome I, Tanida M, Shibamoto T. Effect of hyperpolarization-activated current If on robustness of sinoatrial node pacemaking: theoretical study on influence of intracellular Na^{+} concentration. Am J Physiol Heart Circ Physiol. 2013; 304:H1337–H1351. [PubMed: 23504184]

110. DiFrancesco D. Considerations on the size of currents required for pacemaking. Journal of Molecular and Cellular Cardiology. 2010; 48:802–803.

111. Hilgemann DW. New insights into the molecular and cellular workings of the cardiac Na^{+}/Ca^{2+} exchanger. Am J Physiol Cell Physiol. 2004; 287:C1167–C1172. [PubMed: 15475515]

112. Mitsuiye T, Shinagawa Y, Noma A. Sustained inward current during pacemaker depolarization in mammalian sinoatrial node cells. Circ Res. 2000; 87:88–91. [PubMed: 10903990]

113. Himeno Y, Sarai N, Matsuoka S, Noma A. Ionic mechanisms underlying the positive chronotropy induced by beta1-adrenergic stimulation in guinea pig sinoatrial node cells: a simulation study. J Physiol Sci. 2008; 58:53–65. [PubMed: 18201393]

114. Kharche S, Yu J, Lei M, Zhang H. A mathematical model of action potentials of mouse sinoatrial node cells with molecular bases. Am J Physiol Heart Circ Physiol. 2011; 301:H945–H963. [PubMed: 21724866]

115. Cheng H, Lederer WJ. Calcium sparks. Physiol Rev. 2008; 88:1491–1545. [PubMed: 18923188]

116. Stern MD. Theory of excitation-contraction coupling in cardiac muscle. Biophys J. 1992; 63:497–517. [PubMed: 1330031]

117. Maltsev AV, Maltsev VA, Mikheev M, Maltseva LA, Sirenko SG, Lakatta EG, et al. Synchronization of stochastic Ca^{2+} release units creates a rhythmic Ca^{2+} clock in cardiac pacemaker cells. Biophys J. 2011; 100:271–283. [PubMed: 21244823]

118. Zhou P, Zhao YT, Guo YB, Xu SM, Bai SH, Lakatta EG, et al. Beta-adrenergic signaling accelerates and synchronizes cardiac ryanodine receptor response to a single L-type Ca2+ channel. Proc Natl Acad Sci U S A. 2009; 106:18028–18033. [PubMed: 19815510]

119. Maltsev AV, Yaniv Y, Stern MD, Lakatta EG, Maltsev VA. RyR-NCX-SERCA local crosstalk ensures pacemaker cell function at rest and during the fight-or-flight reflex. Circ Res. 2013; 113:e94–e100. [PubMed: 24158576]

120. Gao Z, Rasmussen TP, Li Y, Kutschke W, Koval OM, Wu Y, et al. Genetic inhibition of Na^{+}-Ca^{2+} exchanger current disables fight or flight sinoatrial node activity without affecting resting heart rate. Circ Res. 2013; 112:309–317. [PubMed: 23192947]

121. Groenke S, Larson ED, Alber S, Zhang R, Lamp ST, Ren X, et al. Complete atrial-specific knockout of sodium-calcium exchange eliminates sinoatrial node pacemaker activity. PLoS One. 2013; 8:e81633. [PubMed: 24278453]

122. Herrmann S, Lipp P, Wiesen K, Stieber J, Nguyen H, Kaiser E, et al. The cardiac sodiumcalcium exchanger NCX1 is a key player in initiation and maintenance of a stable heart rhythm. Cardiovasc Res. 2013

123. Stern MD, Rios E, Maltsev VA. Life and death of a cardiac calcium spark. J Gen Physiol. 2013; 142:257–274. [PubMed: 23980195]

124. Maltsev VA, Maltsev AV, Lakatta EG, Stern MD. Spatial imperfection encodes functional perfection: success and failure of calcium release to propagate regulate pacemaker cell function. Biophys J. 2014; 106(2):319a. (Abstract).

125. Stern MD, Maltseva LA, Juhaszova M, Sollott SJ, Lakatta EG, Maltsev VA. Emergence and synchronization of the "calcium clock" in a 3-dimensional model of a sino-atrial node cell with explicit channel gating. Biophys J. 2014; 106(2):318a. (Abstract).

126. Watanabe Y, Koide Y, Kimura J. Topics on the Na+/Ca2+ exchanger: pharmacological characterization of Na+/Ca2+ exchanger inhibitors. J Pharmacol Sci. 2006; 102:7–16. [PubMed: 16990699]

127. Nivala M, Ko CY, Nivala M, Weiss JN, Qu Z. Criticality in intracellular calcium signaling in cardiac myocytes. Biophys J. 2012; 102:2433–2442. [PubMed: 22713558]

128. Bak, P. How Nature Works: the science of self-organized criticality. New York: Springer-Verlag; 1999.

129. Musa H, Lei M, Honjo H, Jones SA, Dobrzynski H, Lancaster MK, et al. Heterogeneous expression of Ca^{2+} handling proteins in rabbit sinoatrial node. J Histochem Cytochem. 2002; 50:311–324. [PubMed: 11850434]

130. Cummins MA, Devenyi RA, Sobie EA. Yoga for the sinoatrial node: sarcoplasmic reticulum calcium release confers flexibility. J Mol Cell Cardiol. 2013; 60:161–163. [PubMed: 23632045]

131. Prinz AA, Billimoria CP, Marder E. Alternative to hand-tuning conductance-based models: construction and analysis of databases of model neurons. J Neurophysiol. 2003; 90:3998–4015. [PubMed: 12944532]

132. Prinz AA, Bucher D, Marder E. Similar network activity from disparate circuit parameters. Nat Neurosci. 2004; 7:1345–1352. [PubMed: 15558066]

133. Romero L, Pueyo E, Fink M, Rodriguez B. Impact of ionic current variability on human ventricular cellular electrophysiology. Am J Physiol Heart Circ Physiol. 2009; 297:H1436–H1445. [PubMed: 19648254]

134. Kurata Y, Hisatome I, Shibamoto T. Roles of Sarcoplasmic Reticulum Ca^{2+} Cycling and Na^{+}/Ca^{2+} Exchanger in Sinoatrial Node Pacemaking: insights from bifurcation analysis of mathematical models. Am J Physiol Heart Circ Physiol. 2012; 302:H2285–H2300. [PubMed: 22447940]

135. Boink GJ, Nearing BD, Shlapakova IN, Duan L, Kryukova Y, Bobkov Y, et al. Ca^{2+}-Stimulated Adenylyl Cyclase AC1 Generates Efficient Biological Pacing as Single Gene Therapy and in Combination With HCN2. Circulation. 2012; 126:528–536. [PubMed: 22753192]

136. Parker, TS.; Chua, LO. Practical numerical algorithms for chaotic systems. New York: Springer-Verlag; 1989.

137. Oren RV, Clancy CE. Determinants of heterogeneity, excitation and conduction in the sinoatrial node: a model study. PLoS Comput Biol. 2010; 6:e1001041. [PubMed: 21203483]

138. Lang D, Petrov V, Lou Q, Osipov G, Efimov IR. Spatiotemporal control of heart rate in a rabbit heart. J Electrocardiol. 2011; 44:626–634. [PubMed: 21937057]

139. Wolf RM, Glynn P, Hashemi S, Zarei K, Mitchell CC, Anderson ME, et al. Atrial fibrillation and sinus node dysfunction in human ankyrin-B syndrome: a computational analysis. Am J Physiol Heart Circ Physiol. 2013; 304:H1253–H1266. [PubMed: 23436330]

140. Swaminathan PD, Purohit A, Soni S, Voigt N, Singh MV, Glukhov AV, et al. Oxidized CaMKII causes cardiac sinus node dysfunction in mice. J Clin Invest. 2011; 121:3277–3288. [PubMed: 21785215]

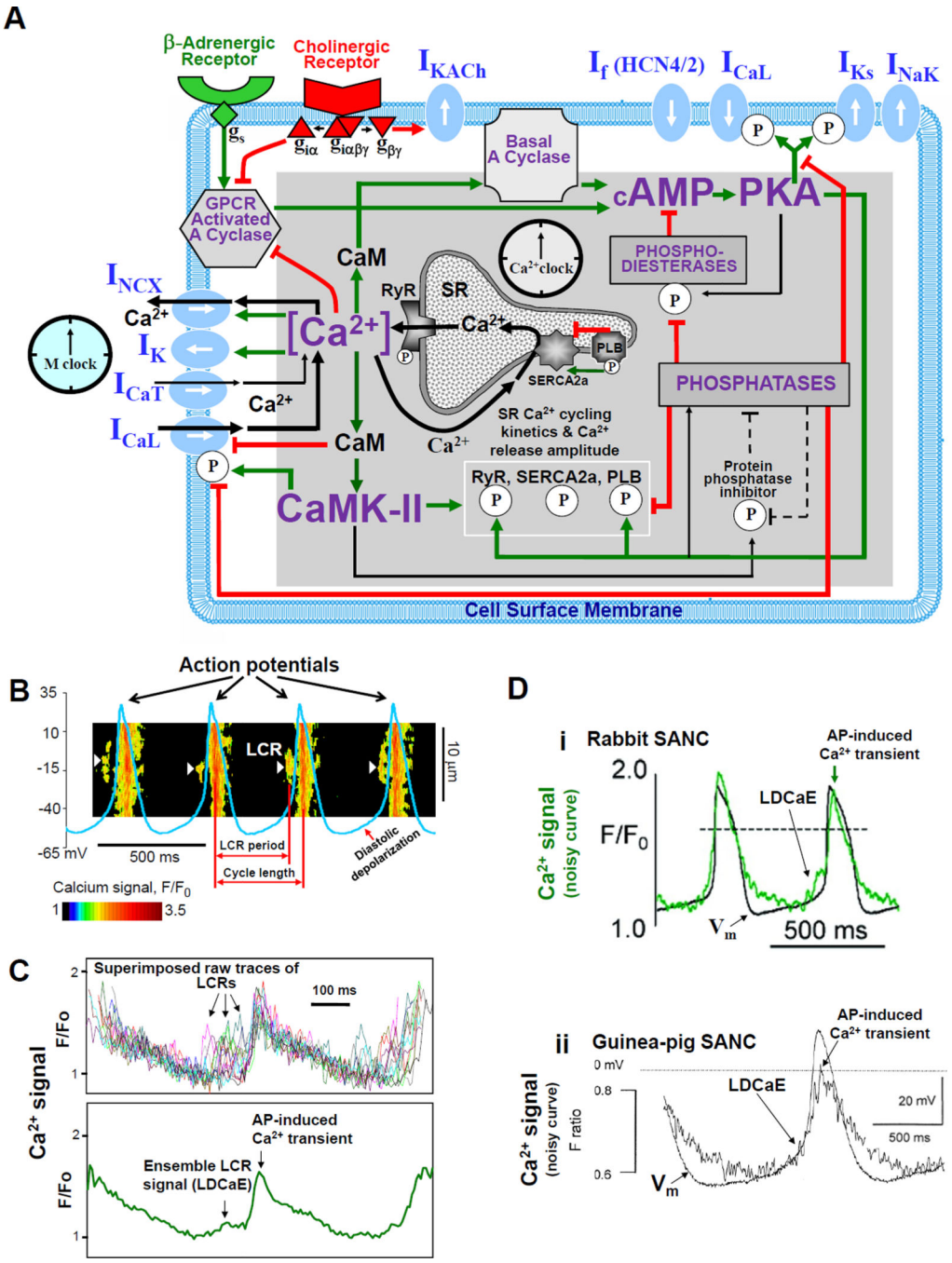

Figure 1.

SA node cell is a coupled-clock system of voltage membrane clock (M-clock) and an intracellular, sarcoplasmic reticulum (SR)-based Ca^{2+} clock. **A**: Schematic illustration of interactions of key molecules comprising the system (PLB = phospholamban). Note that common regulatory factors (purple large lettering) govern the function of both the Ca^{2+}-clock (gray intracellular area) and the M-clock (light-blue cell membrane area with blue labels depicting electrogenic proteins). These common factors act as nodes within the system to couple the function of both clocks activities. The system is balanced as illustrated

by traffic-light-like colors: green arrows designate signaling driving action potential (AP) firing but red lines show suppression, maintaining a given steady-state level of cAMP and protein phosphorylation. G protein-coupled receptors (green and red shapes within the membrane) modulate both the Ca^{2+}-clock and M-clock function via those same crucial signaling nodes of the system. Modified from (11). **B**: Definition of diastolic depolarization, local Ca^{2+} releases (LCRs), LCR period, and cycle length. Line-scan image of LCRs (white arrows) is superimposed with spontaneous APs recorded in rabbit SANC. **C**: upper panel, LCRs imaged by confocal microscopy; lower panel, temporal average of the LCRs creates ensemble LCR signal or Late Diastolic Ca^{2+} Elevation (LDCaE) that precedes AP-induced Ca^{2+} transient. **D**: LDCaE in single SANC of rabbit (sub-panel I, modified from (53)) and guinea-pig (sub-panel ii, modified from (51), published with permission).

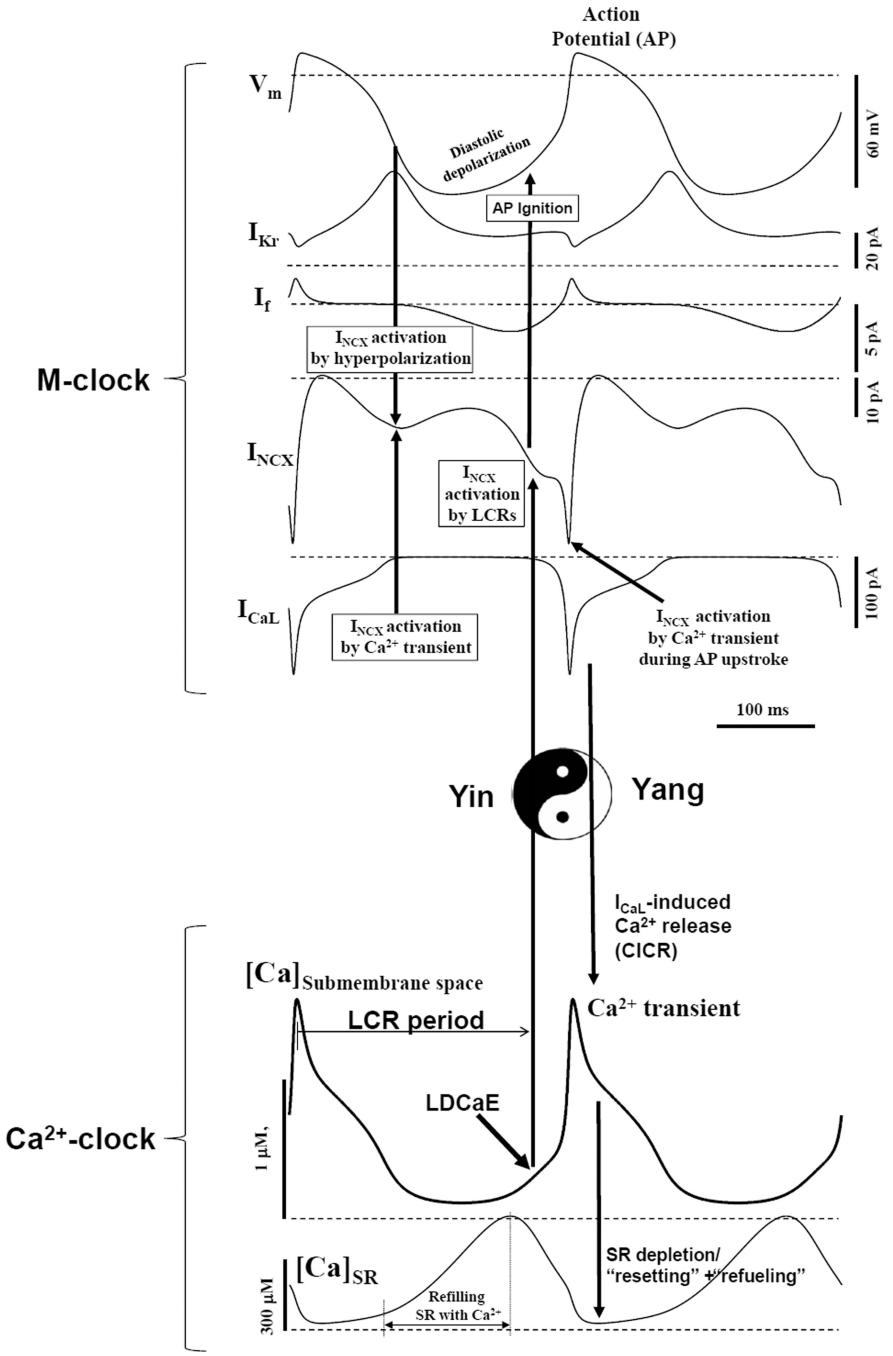

Figure 2.

Maltsev-Lakatta model (10) predicts the "yin-yang" type, synergistic interactions within the coupled-clock system of SANC (see text for details). Modified from (10).

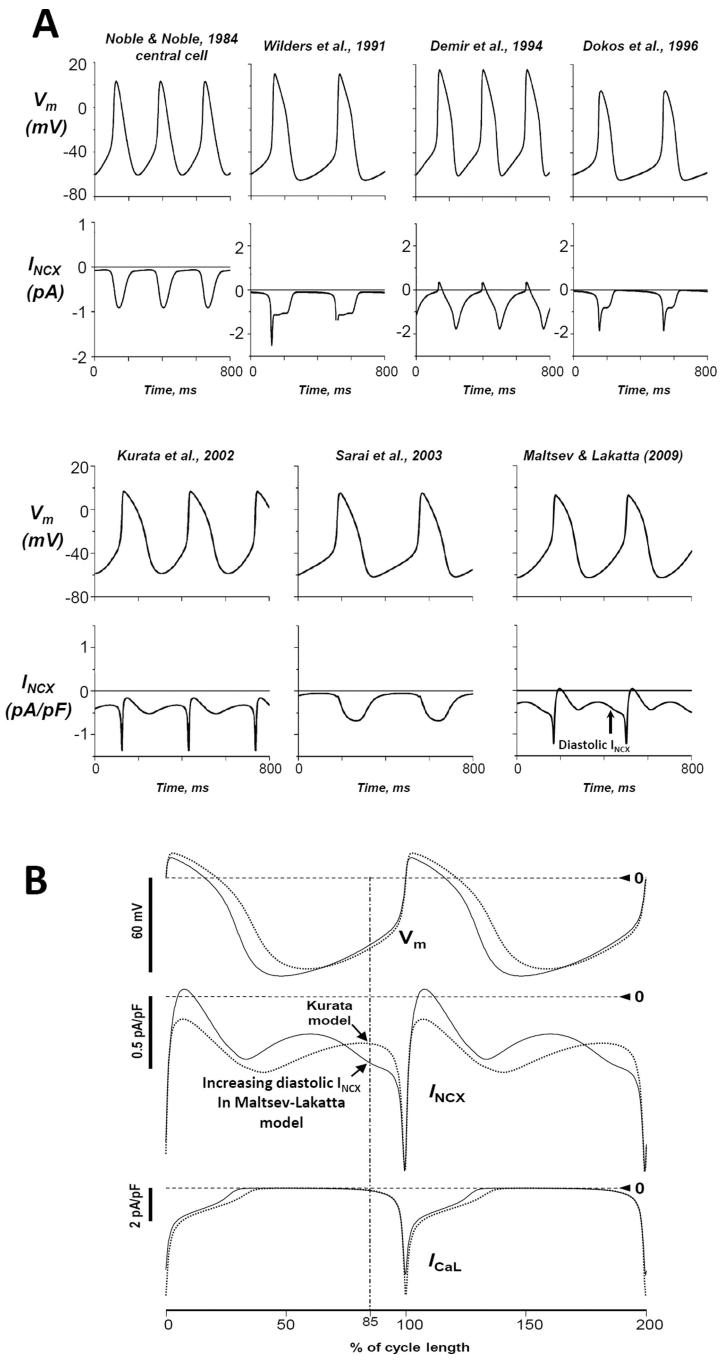

Figure 3.

A: Comparison of I_{NCX} dynamics in different pacemaker cell models. **A:** Only Maltsev-Lakatta model (10), featuring Ca^{2+} clock, exhibits substantial increase in diastolic I_{NCX}. Modified from (44). **B**: In contrast to Kurata et al. model (66) (dotted curves), the ML model (solid curves) exhibits strong increase of inward I_{NCX} during DD clearly before activation of I_{CaL}. The cycle lengths were 307.5 ms and 333 ms for Kurata et al. model and the Maltsev-Lakatta model, respectively. The vertical dash-dot line of 75% of cycle length illustrates approximate timing for I_{CaL} activation. Modified from (10).

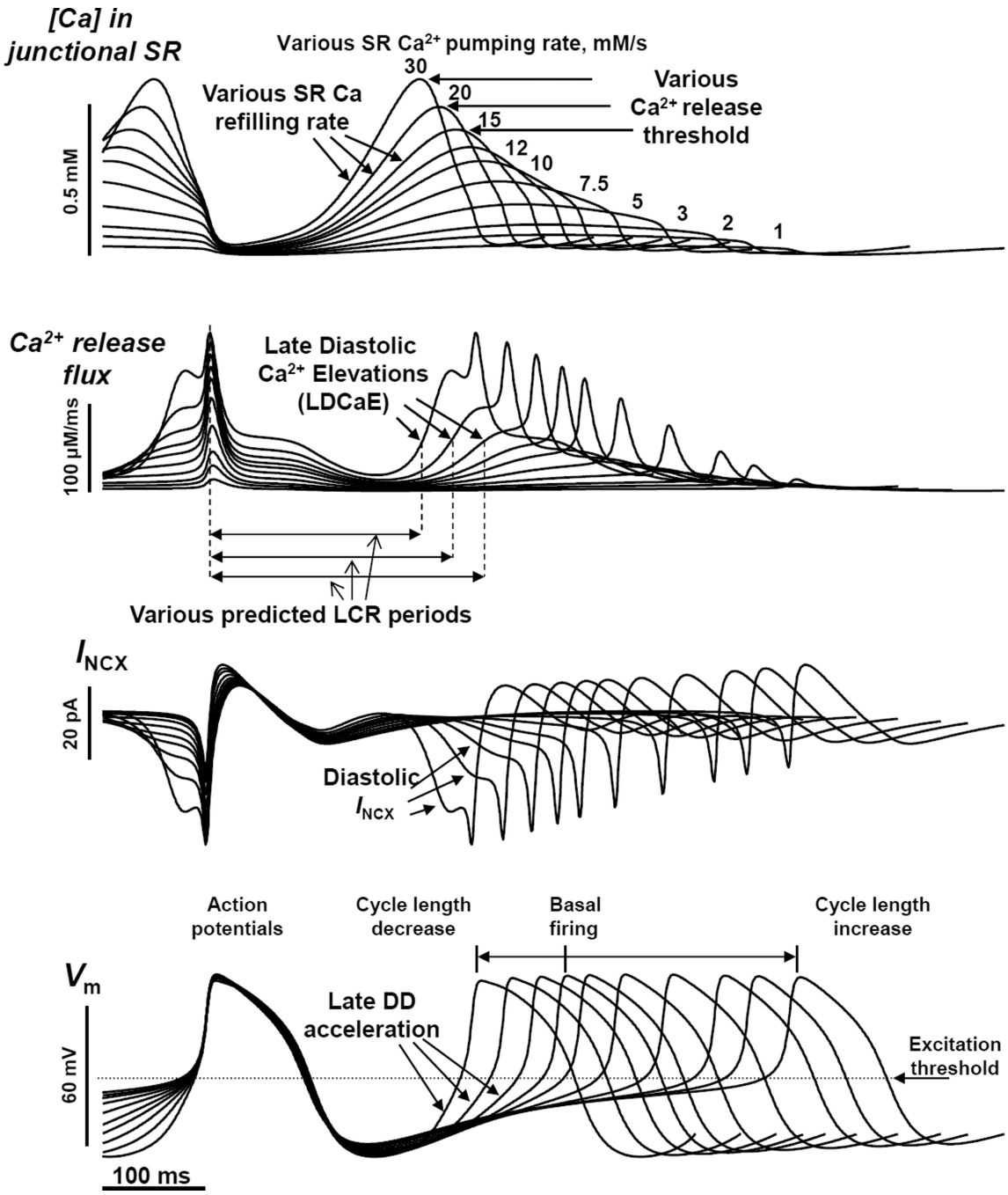

Figure 4.

The Maltsev-Lakatta model (10) predicts the wide range of pacemaker rate modulation via variations in SR Ca^{2+} pumping rate (1 to 30 mM/s), mimicking various degrees of PKA-dependent phospholamban phosphorylation. Modified from (10).

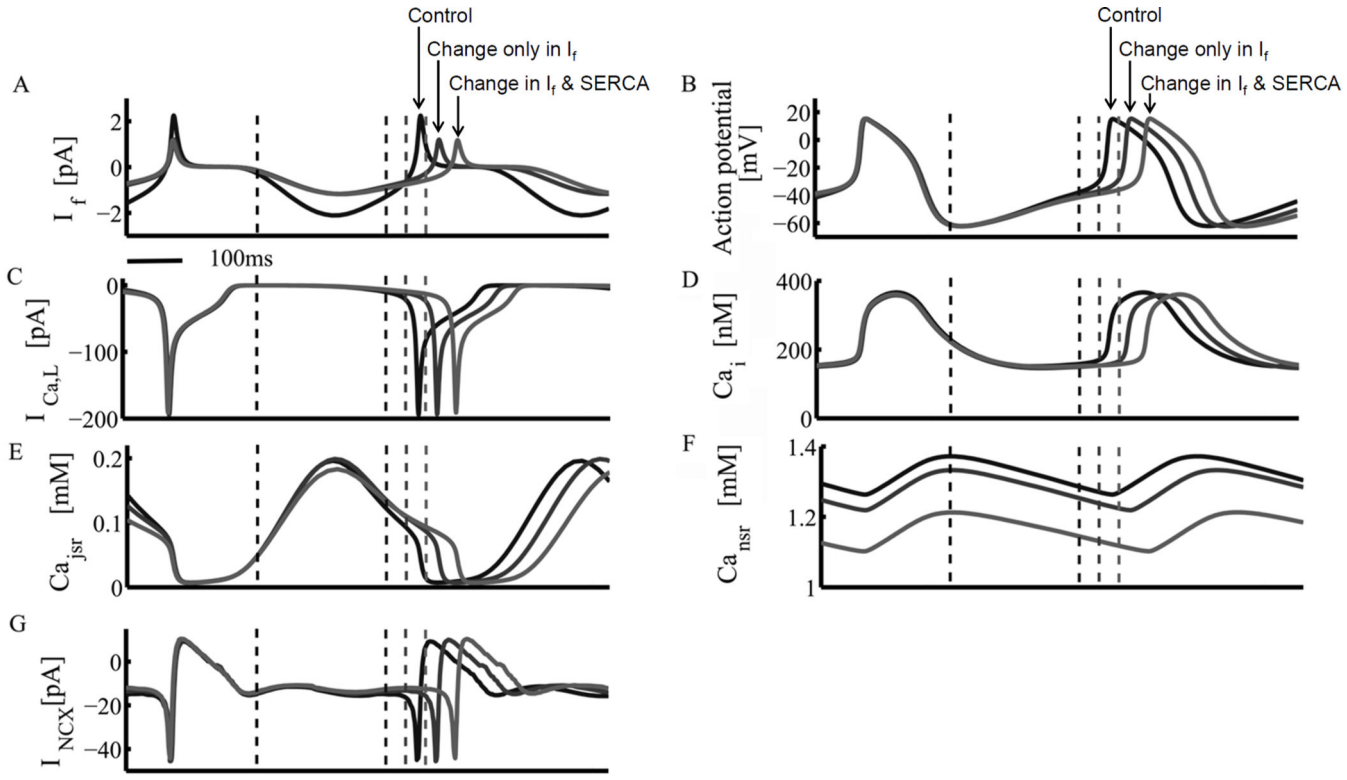

Figure 5.

Effect of a specific reduction of I_f on AP firing rate is mediated via perturbation of both M-clock and Ca^{2+} clock. Simulations using the Maltsev-Lakatta model (10) with integrated mitochondrial Ca^{2+} dynamics predict the effects of IVA on (A) I_f, (B) AP, (C) I_{CaL}, (D) cytosolic Ca^{2+}, (E) junctional, (F) network SR $[Ca^{2+}]$, and (G) sarolemmal I_{NCX}. "Control": model simulations prior to drug. "Change only in I_f": model simulations when only I_f conductance is reduced. "Change in I_f and SERCA": model simulations when both I_f and SR Ca^{2+} pumping (SERCA) parameters were changed. The dashed lines represent the respective diastolic DD phases. From (71).

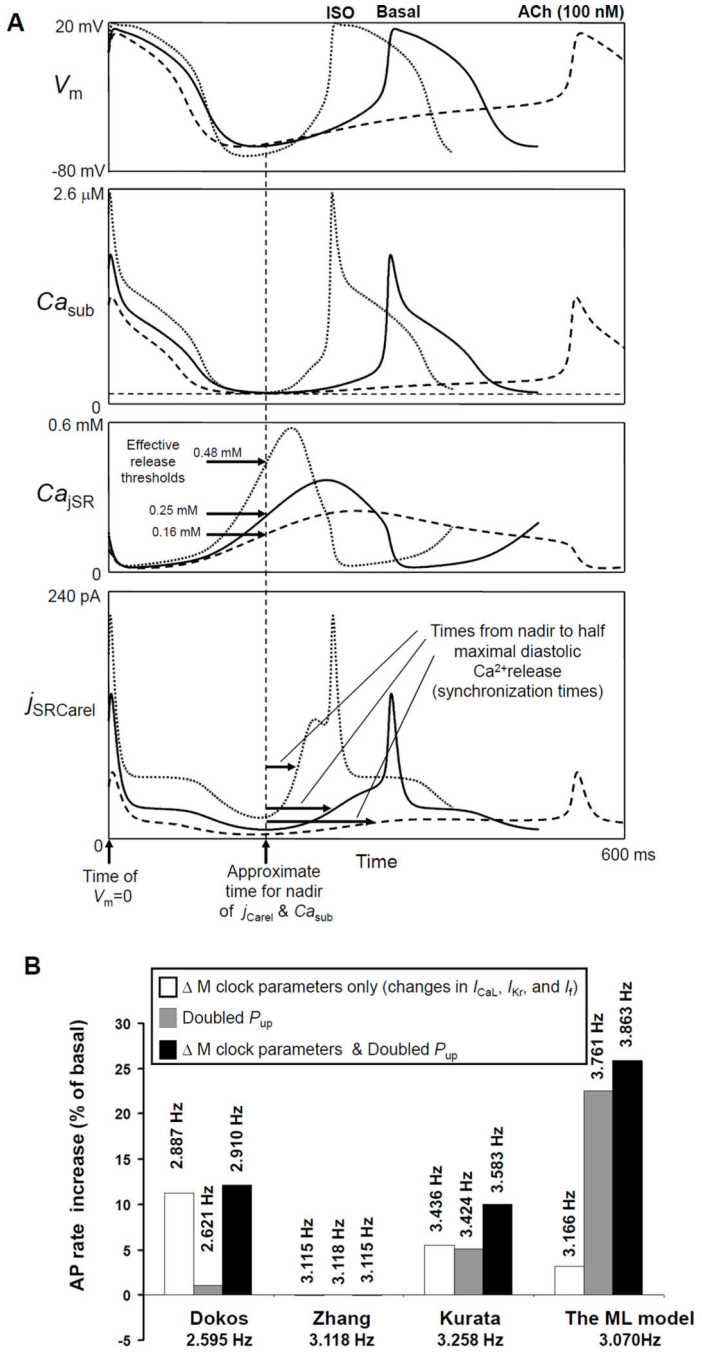

Figure 6.

Numerical modeling of GPCR modulation of AP firing rate in rabbit SANC. **A**: The coupled-clock ML model prediction for the mechanisms of spontaneous Ca^{2+} release in rabbit SANC and their modulation by β-AR (ISO) or ChR (ACh) stimulation. Panels show model simulations of simultaneous changes in membrane potentials (V_m), submembrane [Ca^{2+}] (Ca_{sub}), [Ca^{2+}] in junctional (i.e. Ca^{2+} releasing) SR (Ca_{jSR}), and Ca^{2+} release flux ($j_{SRCarel}$). The Ca^{2+} release becomes more synchronized and occurs earlier in case of ISO, but less synchronized and occurs later in case of ACh, as reflected by times to half

maximum of the diastolic release (in $j_{SRCarel}$ panel). Modified from (43). **B**: Only the ML model predicts the full scale of β-AR stimulation effect reported within the range of 25–30% increase in AP firing rate in rabbit SANC. SANC models, lacking diastolic Ca^{2+} release, substantially underestimate the effect of β-AR stimulation. Models are labeled as follows: "Dokos" (79), "Zhang" (80), "Kurata"(66). Respective bars show the model predictions for the effects of experimentally reported changes of M-clock parameters, doubling the capability of SR Ca^{2+} pumping, P_{up}, or both changes combined. Spontaneous rate change was negligible (within 0.1%) in Zhang et al. model (Note this model has no Ca^{2+} dynamics, i.e. $[Ca^{2+}]$=const). Absolute AP firing rates predicted by the models are shown by labels at the respective bars. Modified from (43).

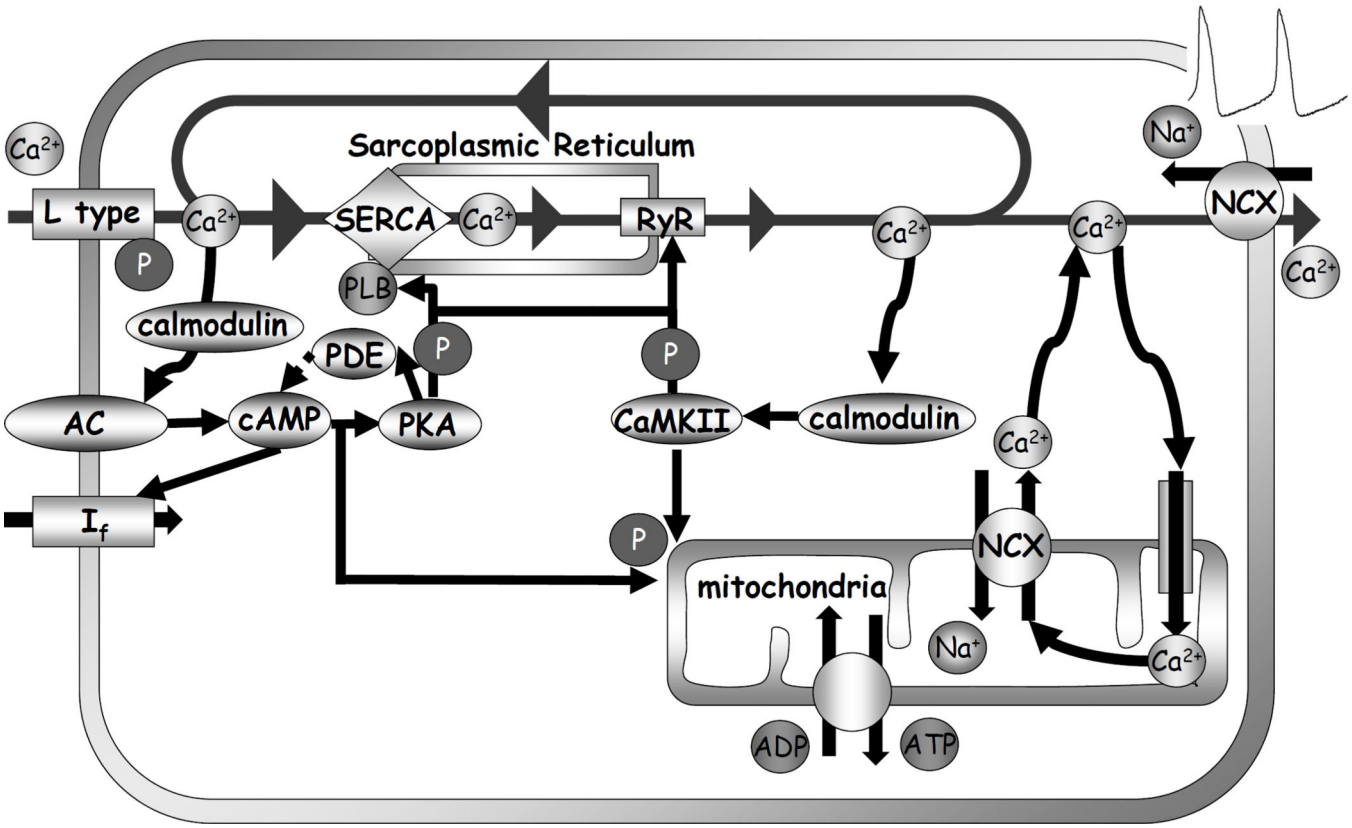

Figure 7.
Schematic illustrations of the coupled clock system that includes a mitochondrial Ca^{2+} flux. From (71).

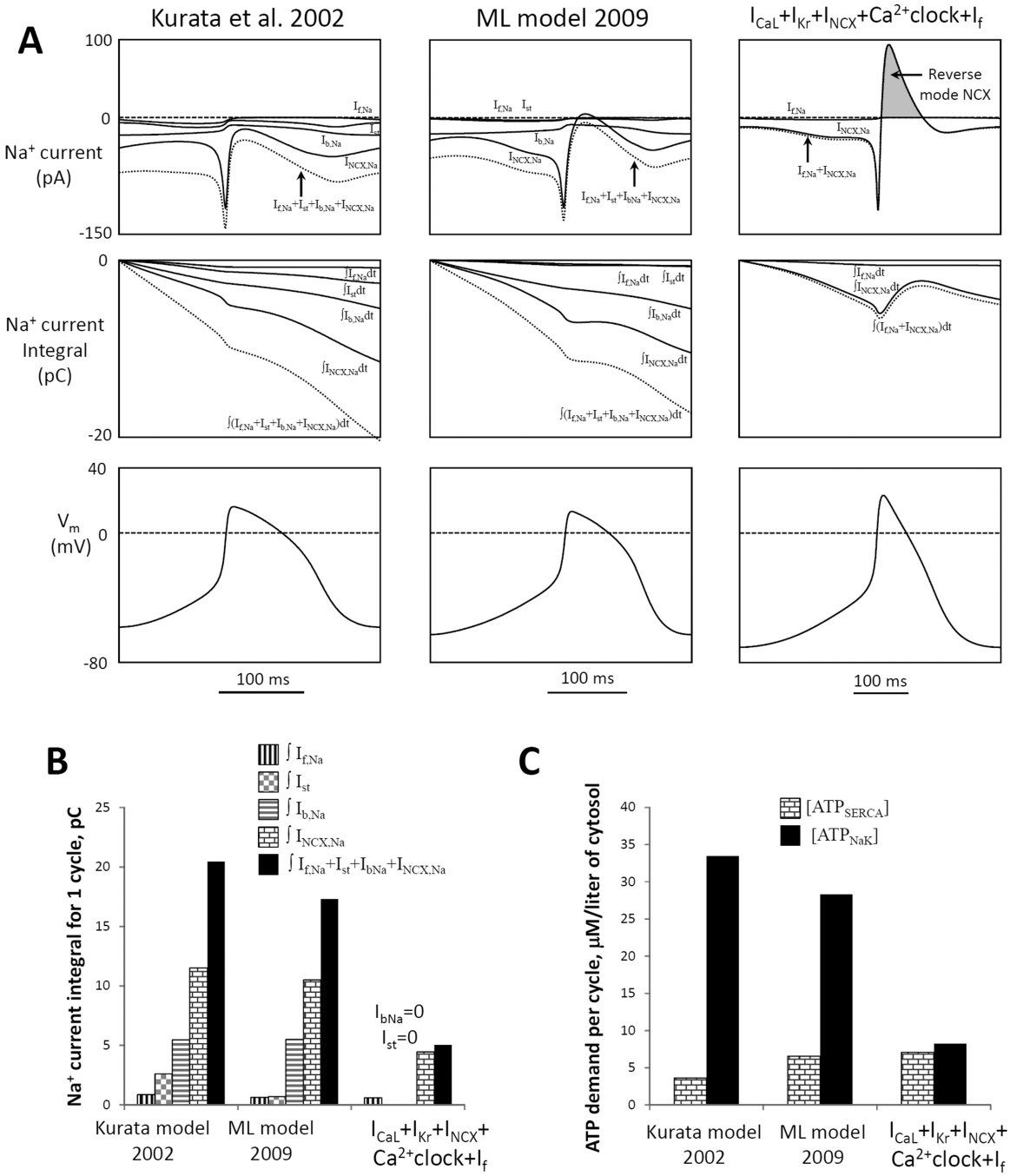

Figure 8.

A flexible and robust pacemaker model with minimal set of components (44) features a small steady-state influx of Na^+ and is expected to be more energy-efficient in terms of Na^+ balance regulation (i.e. requires less ATP-dependent Na^+ extrusion) vs. prior models Kurata et al. (66) and Maltsev and Lakatta (ML) (10). **A**: Top panels show simulations of trans-membrane Na^+ currents via different mechanisms ($I_{f,Na}$, I_{st}, $I_{b,Na}$, $I_{NCX,Na}$) and their sum (dotted lines) in different models for one AP cycle (MDP-to-MDP, bottom panels). Middle panels: respective time-dependent integrals of Na^+ currents of the top panels reflecting Na^+

accumulation (during one AP cycle) in the absence of Na^+ extrusion by ATPases. **B**: Respective integrals of Na^+ currents in panel A calculated for one AP cycle. All three models have cell electric capacitance of 32 pF. C: Cell energy budget to maintain Na^+ homeostasis [ATP_{NaK}] and to pump Ca^{2+} to the SR [ATP_{SERCA}] estimated by three models of SANC. From (44).

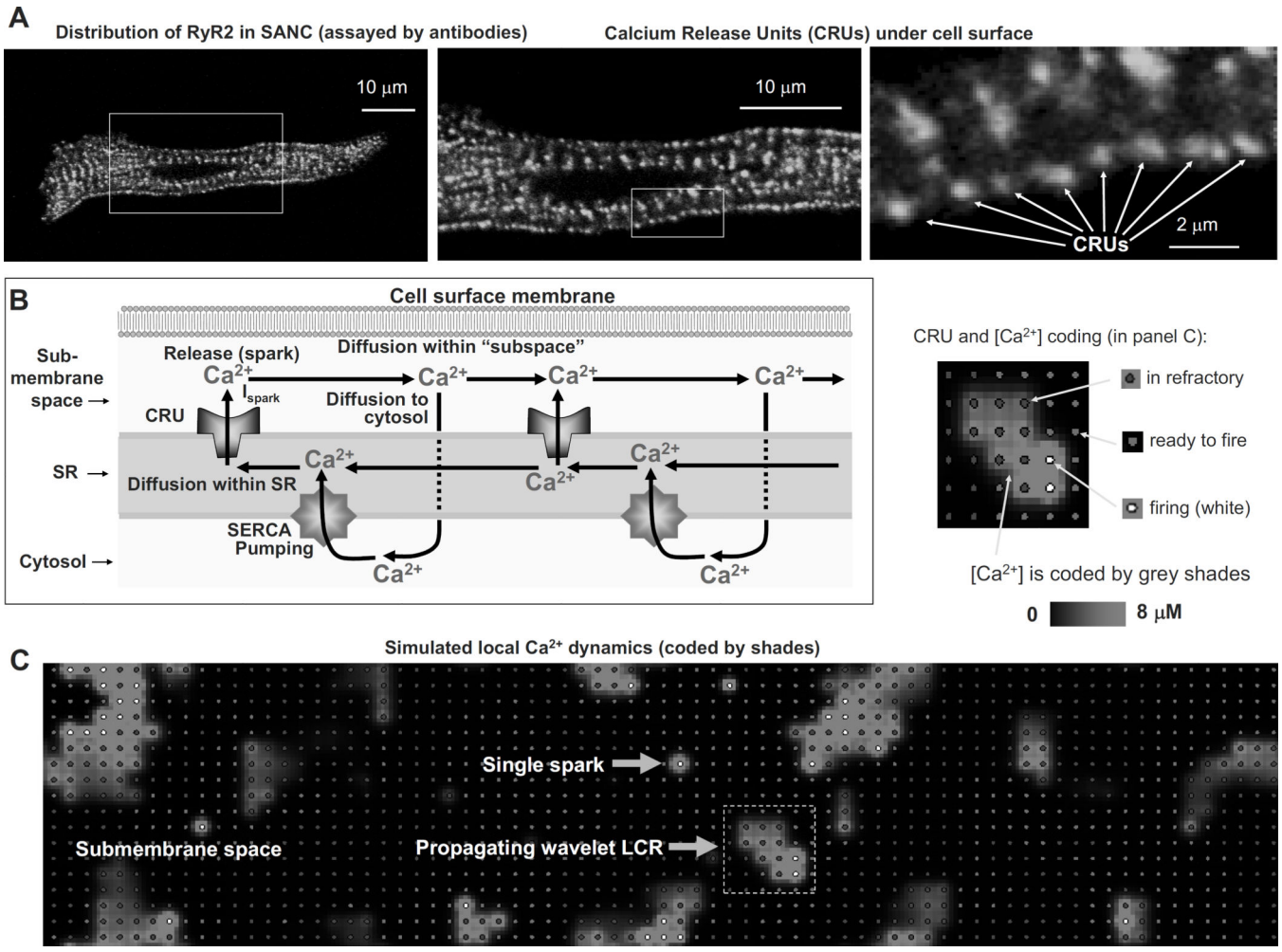

Figure 9.

Development of the numerical model of local Ca^{2+} dynamics in rabbit SANC: Ca^{2+} Release Units, (CRUs) and Ca^{2+} cycling. **A**: RyR clusters, i.e. CRUs, are observed in confocal images of immuno-fluorescence in rabbit SANC under cell surface membrane. **B**: Schematic illustration of local Ca^{2+} cycling through cell compartments (submembrane space, SR, and cytosol) in a new local Ca^{2+} control model of SANC (117, 119). Local Ca^{2+} fluxes in the model are shown by arrows. Ca^{2+} wave travels from left to right. **C**: Instantaneous distributions of local [Ca^{2+}] in the submembrane space predicted by the model: a single Ca^{2+} spark and a wavelet LCRs (propagating from left to right). Inset: Illustration of shade-coding for CRU states and [Ca^{2+}]. Modified from (117).

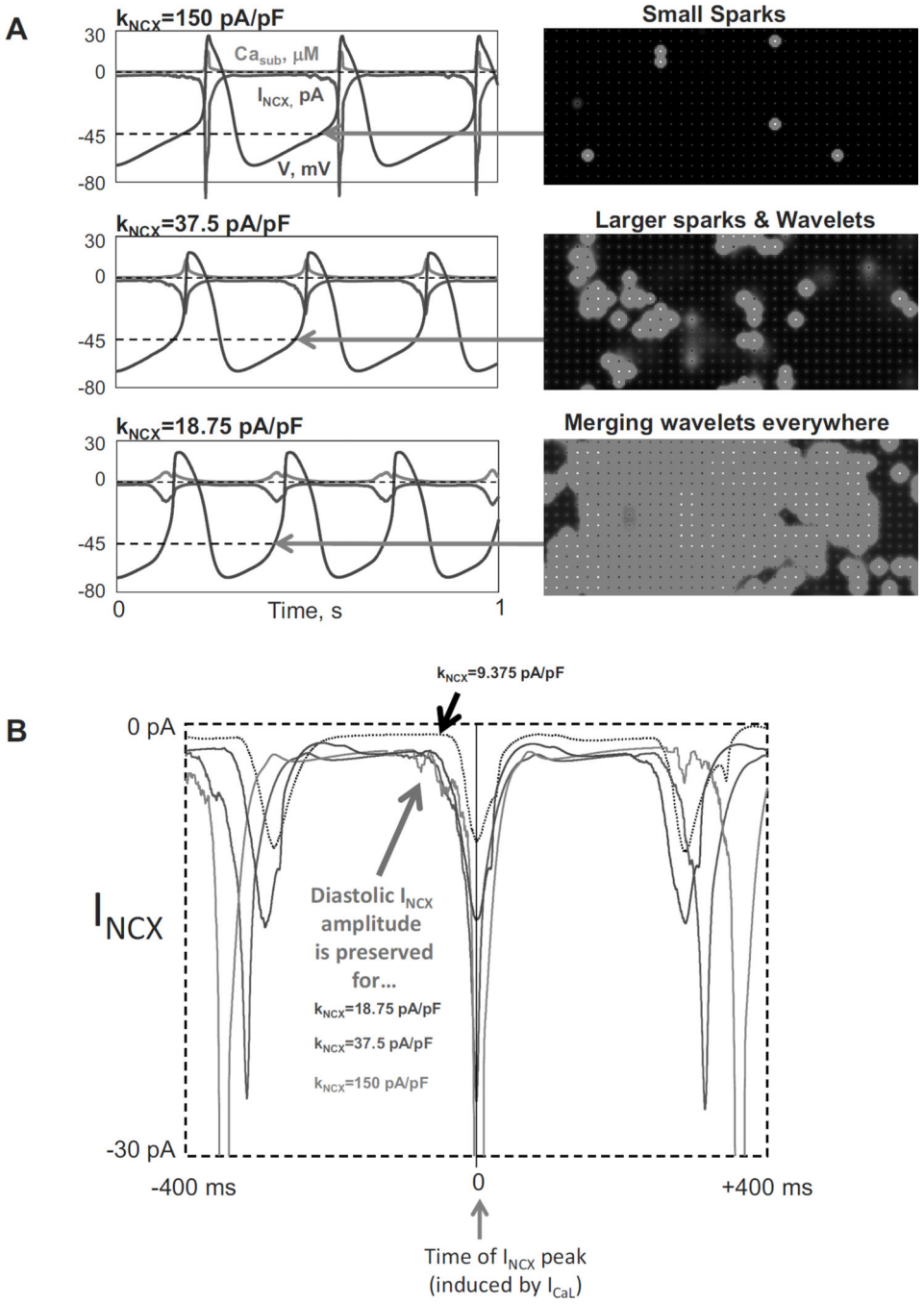

Figure 10.

The magnitude of diastolic I_{NCX} is stabilized by powerful local Ca^{2+} control mechanisms in SANC. **A**: Numerical simulations using a new local Ca^{2+} control model (119) predict dynamics of membrane potential, I_{NCX} and Ca_{sub}, with respective k_{NCX} values (reflecting NCX expression) indicated at the top of each panel. Images on the right illustrate the instantaneous local submembrane $[Ca^{2+}]$ at −40 mV by grey shades, from black (200 nM) to light gray (1000 nM). Ca^{2+} release units, i.e. clusters of RyRs, are shown by dots in mid-grey and white (when firing). **B**: Simulations of the local control model demonstrate that

diastolic I_{NCX} is preserved within a broad range of k_{NCX} variations. The three I_{NCX} traces are the same as in panel A but shown with substantial zoom to clearly demonstrate the I_{NCX} magnitude and dynamics. The traces were synchronized at their peak induced by I_{CaL} via CICR mechanism at the beginning of an AP. I_{NCX} substantially decreased only when k_{NCX} decreased dramatically (dotted curve). From (119).

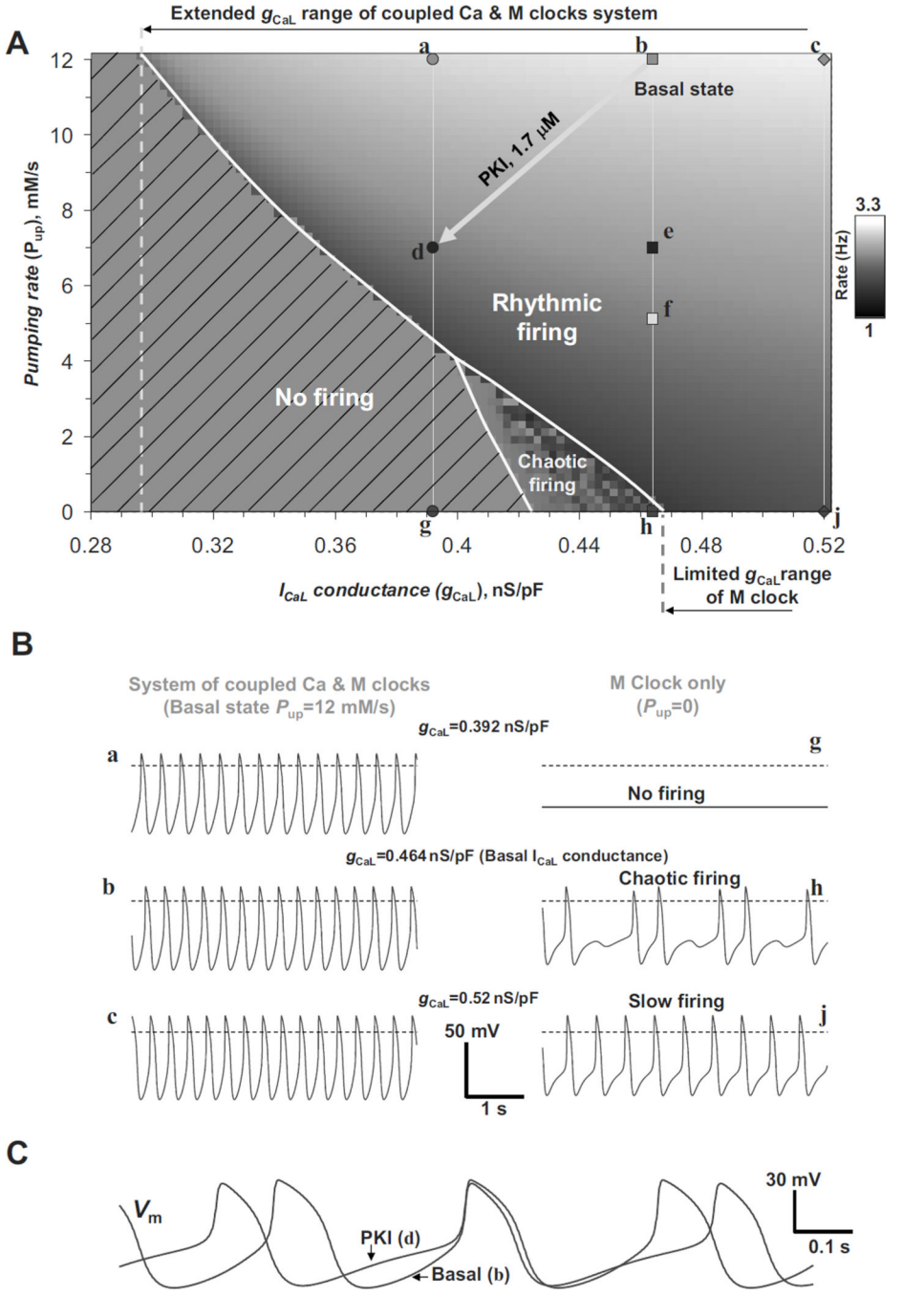

Figure 11.

A: A parametric system analysis ("population-based" modeling) using the ML model (10) with simultaneous variations in I_{CaL} conductance and SR Ca^{2+} pumping rate. The image shows the result of 97(x) × 61 (y) = 5917 simulations (each pixel = 0.0025 nS/pF × 0.2 mM/s). The resultant AP firing rate of the system is illustrated by various grey shades on the right; stripped areas indicate no firing; and mosaic areas indicate chaotic firing. **B**: Simulation traces for specific points of interest in panel A, illustrating more robust system

operation when Ca^{2+} clock is functional. **C**: simulations of the effect of moderate PKA inhibition by 1.7 μM PKI (represented by vector bd in panel A). From (10).

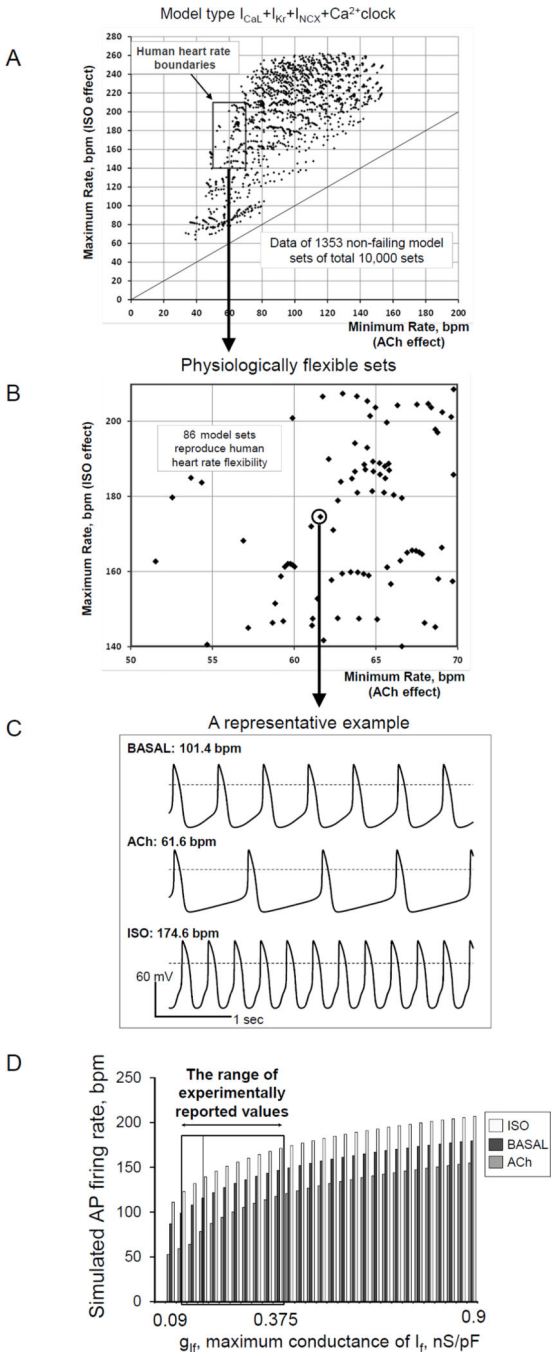

Figure 12.

A: Results of sensitivity analysis (“population-based” modeling) of a 4-parameter model type I_{CaL}+I_{Kr}+I_{NCX}+Ca^{2+}clock. The model type was tested in 10,000 parameter sets. Data points show predictions for maximum and minimum spontaneous AP firing rate achieved with β-AR (ISO) and ChR (ACh) stimulation (along Y and X axis, respectively). **B**: a more detailed representation of all data points within the boundaries of normal human heart operation, including different ages and level of fitness (shown by square in panel A). **C**: an example of APs in basal state and also in ACh test and ISO test. **D**: Results of sensitivity

analysis over a wide range of I_f conductance (g_{If} on X-axis, all other parameters are fixed). When g_{if} is increased beyond the experimentally measured range, both the minimum rate (ACh, grey bars) and the maximum rate (ISO, white bars) increase concurrently, so that the relative rate flexibility is compromised. The double head arrow shows the range of I_f conductance (g_{If}) that simulates the respective range of I_f densities measured experimentally (13). From (44).

Table 1

Major ion currents reported in SA node and SANC of various species.

Group of currents	Ion current	References
Voltage-gated Na^+ current	I_{Na} (absent in primary SANC)	(12, 13)
Voltage-gated Ca^{2+} currents (I_{Ca}= I_{CaL}+I_{CaT})	I_{CaL}, High voltage-activated, L-type Ca current	(14)
	I_{CaT}, Low voltage-activated, T-type Ca current	(14–16)
Voltage-gated K^+ currents ($I_{4\text{-}AP}$=I_{to}+I_{sus} and I_K=I_{Kr}+I_{Ks})	I_{to}, 4-AP sensitive transient K^+ current	(17, 18)
	I_{sus}, 4-AP sensitive sustained outward K^+ current (the sustained part of initially discovered I_{to} or $I_{4\text{-}AP}$)	(18, 19)
	I_{Kr}, the rapidly activating component of I_K exhibiting strong inward rectification (mouse, rat, guinea pig, rabbit)	(20, 21)
	I_{Ks}, the slowly activating component of I_K exhibiting only weak rectification (guinea pig, pig)	(21)
	I_{K1}, inwardly rectifying K^+ current (mouse, rat, and monkey)	(22)
Voltage-gated monovalent cation non-selective currents	Hyperpolarization-activated, “funny” current, I_f or I_h	(23–25)
	Sustained inward current I_{st} (non-selective)	(26)
ACh-activated K^+ current	I_{KACh}	(27)
Background and ion transporter currents	Store-operated Ca^{2+} current (mouse)	(28)
	Background Na^+ current, $I_{b,Na}$	(29)
	Na^+/K^+ pump current, I_{NaK} or I_p	(30, 31)
	Na^+/Ca^{2+} exchanger current, I_{NaCa} or I_{NCX}	(32–36)
	Cl^- current, I_{Cl} Present in about one third of rabbit SANC	(37)